HIGH-PRECISION MICROPIPETTE THERMAL SENSOR FOR MEASUREMENT OF THERMAL CONDUCTIVITY OF CARBON NANOTUBES THIN FILM

Ramesh Shrestha, B.E.

Thesis Prepared for the Degree of

MASTER OF SCIENCE

UNIVERSITY OF NORTH TEXAS

August 2011

APPROVED:

Tae-Youl Choi, Major Professor
Sandra Boetcher, Committee Member
Yong X. Tao, Committee Member and Chair of the Department of Mechanical and Energy Engineering
Costas Tsatsoulis, Dean of the College of Engineering
James D. Meernik, Acting Dean of the Toulouse Graduate School

Shrestha, Ramesh. High-precision micropipette thermal sensor for measurement of thermal conductivity of carbon nanotubes thin film. Master of Science (Mechanical and Energy Engineering), August 2011, 64 pp., 3 tables, 25 illustrations, references, 41 titles.

The thesis describes novel glass micropipette thermal sensor fabricated in cost-effective manner and thermal conductivity measurement of carbon nanotubes (CNT) thin film using the developed sensor. Various micrometer-sized sensors, which range from 2 μm to 30 μm, were produced and tested. The capability of the sensor in measuring thermal fluctuation at micro level with an estimated resolution of ±0.002^{o}C is demonstrated. The sensitivity of sensors was recorded from 3.34 to 8.86 μV/^{o}C, which is independent of tip size and dependent on the coating of Nickel. The detailed experimental setup for thermal conductivity measurement of CNT film is discussed and 73.418 W/m^{o}C was determined as the thermal conductivity of the CNT film at room temperature.

ACKNOWLEDGEMENTS

First and foremost I would like to express my sincere gratitude towards Dr Tae-Youl Choi for his guidance and support throughout my entire work. I greatly appreciate for his enthusiasm and confidence towards me and for his invaluable comments and suggestions wherever necessary for completing my research work successfully.

I am deeply indebted to Mr. Anchal Sondhi, Ph.D. student in Department of Material Science at University of North Texas for his assistance in thin film coating using physical vapor deposition machine (PVD) to prepare the thermal sensors.

I would like to thank Mr. Kyungmin Lee, Ph.D. student in Department of Physics at University of North Texas for his help in preparing the samples for the experiments. I would also like to thank the staff in the Physics workshop and in particular Mr Kurt Weihe, Physics Instrument Toolmaker in Department of Physics, for his assistance in building parts for the equipment for my research. I wish to acknowledge Center for Nanoscale Mechantronics and Manufacturing of the 21st Century Frontier Research Program for providing the financial support to this research.

Lastly but not the least, I wish to express my sincere thanks to Mr. Sanjay Gurung for helping me to prepare this thesis and also I would like to thank all those people who helped me directly or indirectly in this work.

TABLE OF CONTENTS

Page

ACKNOWLEDGEMENTS iii

LIST OF TABLES vi

LIST OF ILLUSTRATIONS vii

NOMENCLATURE x

Chapters

1. INTRODUCTION 1
   - 1.1 Objectives 4
   - 1.2 Organization of the Thesis 4

2. LITERATURE REVIEW 6
   - 2.1 Heat Conduction 6
   - 2.2 Steady-State Methods 8
     - 2.2.1 Guarded Parallel Plate 8
     - 2.2.2 Radial Heat Flow Method 9
     - 2.2.3 3-ω Method 11
   - 2.3 Transient Methods 13
     - 2.3.1 Transient Hot Wire Technique 14
   - 2.4 Thermocouple Based Method 15
     - 2.4.1 Thermocouple Circuit 18
     - 2.4.2 Cold Junction Compensation 20
   - 2.5 Natural Convection 24

3. METHODOLOGY AND MATERIALS 27
   - 3.1 Micro-pipette Thermal Sensor 27
     - 3.1.1 Fabrication of Pipette Sensor 27

3.1.2 Calibration 31
3.2 Measurement of Thermal Conductivity of CNT Film 34
3.2.1 CNT Film Preparation 35
3.2.2 Experimental Setup 38
3.2.3 Laser Power Measurement 44
4. RESULTS AND DISCUSSIONS 46
4.1 Calibration of Pipette Sensor 46
4.2 Thermal Conductivity Measurement of CNT Film 51
5. CONCLUSIONS AND RECOMMENDATIONS 56
5.1 Conclusions 56
5.2 Recommendations 57
REFERENCES 59

LIST OF TABLES

Page

Table 2.1 Some common type of thermocouple commercially available 17

Table 4.1 Seebeck coefficients obtained from the calibration..... 50

Table 4.2 Summary of the measurement to determine the thermal conductivity of CNT film 55

LIST OF ILLUSTRATIONS

Page

Figure 2.1 Schematic diagram of guarded parallel plate 9

Figure 2.2 A schematic of cylindrical shell showing the elemental control volume for radial heat conduction 10

Figure 2.3 Three-omega method for thermal conductivity measurement 13

Figure 2.4 Schematic showing the seebeck effect..... 16

Figure 2.5 Schematic of thermocouple circuit..... 19

Figure 2 6 Thermo electric bridge method 22

Figure 2.7 Schematic of thermoelectric refrigeration method 23

Figure 2.8 Schematic of heated oven method for cold junction compensation... 24

Figure 3.1 Fabrication steps of pipette thermal sensor: (a) an empty pipette with less than 1 μm opening; (b) a schematic outline of the filled pipette with a solder alloy and coated nickel; (c) after filling with a solder alloy and beveling; (d) after physical vapor deposition (PVD) thin film coating of nickel and silver; (e) a prototype micropipette thermal sensor. 28

Figure 3.2 Image of the setup used for beveling of the micropipette with BV-10 micropipette beveler. 29

Figure 3.3 SEM image of beveled tip of micropipette prior to PVD deposition. .. 30

Figure 3.4 Schematic of calibration chamber 32

Figure 3.5 Image of the calibration chamber with insulation to maintain at a constant temperature. 32

Figure 3.6 Calibration of sensors varying in tip diameters from 4 to 30 microns that were produced with the same PVD conditions. 34

Figure 3.7 Steps in preparing CNT film on polycarbonate substrate. 37

Figure 3.8 SEM image showing the thickness of the CNT film. 38

Figure 3.9 Experimental setup for the thermal conductivity measurement of CNT film with micropipette sensor. 39

Figure 3.10 Measurement of temperature with pipette sensor. (a) CNT film at focal plane. (b) laser shined at the center of the film, (c) pipette sensor at position 1 and (d) pipette sensor at position 2. 41

Figure 3.11 Lab view program used for controlling the voltage recording of the nano voltmeter. 42

Figure 3.12 Schematic model showing the heat distribution in radial direction due to the laser shined at the center of the CNT film. It was measured and verified that for r> 25 μm surface temperature equals the temperature of surrounding. 43

Figure 3.13 Calibration of image taken with CCD camera with SEM image (a) SEM image (b) CCD camera image. 44

Figure 4.1 Calibration of sensors varying in tip diameters from 4 to 30 microns that were produced with the same PVD conditions (Power = 300 W, Deposition time = 1 hr). 47

Figure 4.2 Calibration of sensors varying in tip diameters from 3.75 to 4.77 microns that were produced with the same PVD conditions (Power = 250 W, Deposition time = 45 mins). 48

Figure 4.3 Calibration of sensors varying in tip diameters from 10 to 12 microns that were produced with the same PVD conditions (Power = 200 W, Deposition time = 30 mins)..... 48

Figure 4.4 Calibration of sensors varying in tip diameters from 3 to 7 microns that were produced with the same PVD conditions (Power = 250 W, Deposition time=1 hr). 49

NOMENCLATURE

A	Surface area perpendicular to heat flow [m^2]
C	Constant
CCD	Charge-couple device
CNT	Carbon nanotube
D	Diameter of cylinder [m]
E	Electron energy
e	Electronic charge
g	Gravitational acceleration [m/s^2]
Gr_x	Grashof number
h	Convective heat transfer coefficient [W/m^2K]
K	Boltzmann constant
k	Thermal conductivity [W/m°C]
Nu_x	Nusselt number
Pr	Prandtl number
PVD	Physical vapor deposition
q	Heat production per unit time per unit length [W/m]
$\dot{Q}$	Heat flow [W]
r	Radius [m]
Ra_x	Rayleigh number

RSS	Root sum square
S	Seebeck coefficient [μV/°C]
SEM	Scanning electron microscope
T	Temperature [°C]
T_f	Averaged fluid temperature [K]
T_s	Surface temperature of sample [K]
T_{Tip}	Sample surface temperature [°C]
T_{Ref}	Reference junction temperature [°C]
V_{Gage}	Voltage output [V]
x	Thickness/characteristic length [m]
α	Thermal diffusivity [m^2/s]
β	Volumetric coefficient of expansion [1/K]
ζ	Fermi energy
ν	Kinematic viscosity [m^2/s]
λ	Mean free path of the conduction electron
ω	Omega

CHAPTER 1

INTRODUCTION

Micro-level thermal sensing is useful in determining the thermal transport properties of thin films and studies of biological activities occurring at a cellular level. For example, temperature sensing in individual cells can provide important data for thermal therapy or detection of cancer [9], metabolomic activity [6], thyroid gland disease diagnosis [1] and heat induced denaturation of DNA and proteins [12]. In addition, with increasing emphasis on micro/nano-technology, research interests have been focused on the investigation of micro/nano-structured materials, devices and their properties. Emerging need in reducing the size of electronic devices and integrated micro/nano-electro-mechanical systems (MEMS and NEMS) provides rationale for the growing importance of the scientific research and technological advancement in micro/nano-technology. In the design of micro-electronic device, a particular issue that needs to be addressed is the change of thermal transport properties of the components in micro/nano scale [5]. A thorough understanding and knowledge of thermal behavior in micro devices is critical in controlling their performance and stability.

Carbon nanotubes (CNT hereafter) have novel properties with many applications in nanotechnology, which have made it a subject of intense research. They exhibit extraordinary strength, electrical properties, and thermal

properties and therefore have wide applications in electronic and optoelectronic, biomedical, energy and other fields of material sciences. For example, CNTs are used in displays applications (CNT field emission displays) because they are excellent sources of electron beams [32]. Due to the special nanostructure, excellent biocompatibility and good conductivity, CNTs are employed to develop various electrochemical sensors. They have applications in architectural field to strengthen the tensile properties of building materials and there are researches in process for building body armor made of CNT fibers. Therefore the determination of transport properties in micro level will help understand the structure and conduction mechanisms in the material and would benefit both academic research and numerous industrial applications of CNTs.

The study of physical phenomena at a micro scale is made possible today with the development of atomic force microscopy, scanning probe microscopy and ultrafast light sources which have enabled the measurement of thermal, mechanical, chemical, electronic, optical, and acoustic properties of materials [2]. However thermal conductivity of a very thin films with thickness $t < 1$ μm have been seldom measured due to the experimental problems [27]. According to Volklein [27] various plate method for determination of thermal conductivity of thin film are not useful as the thermal resistance of the interfaces between film and plates or heat sinks rather than the thermal conductivity of the film is the dominating measuring quantity. The other problem in the measurement of the thermal conductivity is aroused when large temperature sensors are used where

the relative loss of heat by sensor may be large than the heat flow in thin films. The solution to this problem is to employ a laser point source for heating instead of using bulky heating strip that are much wider than the film thickness and avoid thermal resistance of the interfaces between heating strip and film. In addition, the use of a micro scale thermal sensor with high sensitivity and resolution should be employed for measuring the temperature change accurately and avoid the loss of heat from the sensing tip. Such thermocouple probes based on a glass micropipette for the measurement of thermal responses has been demonstrated [8, 13]. However, they were unable to provide meaningful temperature data that would validate the accuracy and resolution of the sensor [13]. In addition, the fabrication technique is intricate, requiring several processes [13] or drawing of a micro platinum wire [8] inside a micro-capillary tube. Gold and platinum as thermocouple materials were used [8, 14]. These materials are expensive and generate relatively small thermo power (i.e., a low level of thermoelectric voltage signals).

In this thesis, the fabrication of a novel glass micropipette thermal sensor is described and a new method for the determining the thermal conductivity of thin film of CNT at room temperature is presented. The micropipette thermal sensors were fabricated such that different tip sizes were produced with varying coating conditions during physical vapor deposition (PVD hereafter). Then the micropipette thermal sensors were calibrated individually using a constant-temperature water bath chamber and was used to measure the temperature

difference at two spots, which were 10 to 20 μm apart, on a 100 nm thick CNT film. The measurement and calculation is detailed in chapter 3.

1.1 Objectives

The main objective of the research is to develop a novel glass micro-pipette thermal sensor in a cost effective method and use it to measure the thermal conductivity of thin film of CNTs and demonstrate the capability of measuring the temperature fluctuation in cellular level.

Specific objectives

- To fabricate the micro-pipette thermal sensor using nickel and lead free solder wire (tin).
- To calibrate the fabricated sensor.
- To compare the sensitivity of the sensors produced by different coating conditions during PVD sputtering.
- To measure the thermal conductivity of thin film of Carbon-nanotubes deposited on polycarbonate substrate.

1.2 Organization of the Thesis

Chapter 2 presents the results of the literature research. This chapter describes the thermal conductivity measurement techniques. The steady state method for the measurement of the thermal conductivity is described in more details as this technique is used to determine the thermal conductivity of the CNT

thin film. Chapter 2 details the equation used for the thermal conductivity calculation and discusses the principles of thermocouple and describes the assumption made during the measurement of the temperature.

Chapter 3 deals with the methods and materials used in the experiment. It discusses the process for the fabrication of the sensor, calibration of the sensor, instruments used for data recording, experimental setup and data collection procedure during the experiment.

Chapter 4 discusses the results of the calibration of sensors, and provides the experiment result for the thermal conductivity of the CNT film.

Chapter 5 concludes the thesis with a summary and providing guidelines for possible future extensions of this work.

CHAPTER 2

LITERATURE REVIEW

This chapter briefly discusses the results of the literature research. Two techniques, steady state and transient methods, used for measuring thermal conductivity of materials and thin film are discussed. Since the steady state method is used in the research, literature related to this is discussed in more details. The sensors developed are thermocouples made of nickel and tin alloy and were calibrated individually as each sensor differs in tip size even though the physical vapor deposition (PVD hereafter) coating condition was same for one batch of sensors. The calibration was performed using the steady state water bath. Theory related to thermocouple, calibration and measuring principle are also discussed in detail in this chapter.

2.1 Heat Conduction

Thermal conduction is the mechanism whereby energy is transported through a solid medium due to a temperature difference. The principle of thermal conduction is stated by Fourier's law according to which the heat transfer by conduction per unit area (heat flux) in a particular direction is proportional to the negative of local temperature gradient in that direction [20]. The proportionality constant in this law is known as thermal conductivity and is denoted by the

symbol k. For a one-dimensional heat conduction with temperature varying in x direction only, heat flow is obtained by equation,

$$\dot{Q} = -k\ A\ \frac{dT}{dx} \tag{2.1}$$

where: $\dot{Q}$ = heat flow [W]

k = thermal conductivity [W/m°C]

A = surface area perpendicular to heat flow [m^2]

$\frac{dT}{dx}$ = temperature gradient along x direction [°C/m]

In cylindrical coordinates, with temperature varying in radial direction only, the equation for heat flow is written as

$$\dot{Q} = -k\ A\ \frac{dT}{dr} \tag{2.2}$$

where: $\frac{dT}{dr}$ = temperature gradient along r (radius) direction[°C/m]

There is no particular thermal conductivity measurement method universally accepted for thin films as each class of thin films present unique set of properties and obstacle to overcome during the experiment. However from the literature research, it was found that researchers have been following two techniques, steady state and transient techniques to determine the thermal conductivity and diffusivity which is discussed in detail below.

2.2 Steady-State Methods

Steady-state methods for measuring the thermal conductivity provide the direct evaluation of the thin film thermal conductivity and are based on Fourier's law of heat conduction. Most of the techniques employ infinite parallel slab or cylinders as sample model and the mathematics for determining the thermal conductivity is simplified by reducing the heat transfer problem to a one-dimensional problem.

2.2.1 Guarded Parallel Plate

The guarded parallel plate method is used for measuring thermal conductivity of solids that are poor conductors of heat and can be made into a slab. The principle of this method is straightforward. The sample is placed in a narrow gap between two parallel plates: upper heater and a lower plate. The upper plate is surrounded by a guard plate whose temperature is maintained at the same temperature as the upper plate in order to reduce the heat loss from the upper surface of the upper plate and to ensure a one dimensional heat transfer at the edges of the sample. A small amount of heat is generated in the upper plate and is transported through the sample to the lower plate (sink) producing a small temperature difference across the sample surfaces. After reaching the steady state which is determined by the stable temperatures of the upper and lower plate, the heat flux across the sample and the temperatures at the surfaces of the upper and lower plates are measured precisely and then after thermal conductivity of the sample can be deduced from the simple linear form of

Fourier's law of heat conduction as mentioned in equation 2.1. The schematic diagram of the guarded parallel plate is shown in figure 2.1 [46].

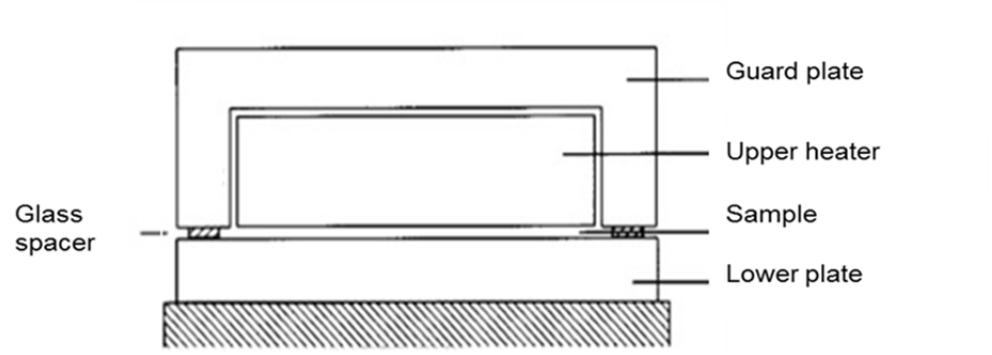

Figure 2.1 Schematic diagram of guarded parallel plate.

The main advantage of this technique is the precise measurements of the heat generation and surface temperatures which can be used for the direct evaluation of thermal conductivity. However in micro scales the fabrication of the heater on the sample surface is a difficult process and there is always spurious heat loss between heater and sample due to unavoidable contact resistance between irregular surfaces of heater and sample.

2.2.2 Radial Heat Flow Method

This method is most commonly used for measuring the thermal properties of powdered or granular material. The principle is simple which is based on the Fourier's conduction for a cylindrical shell.

A sample is prepared in cylindrical shape whose diameter is indefinitely larger than line or cylindrical heat source used for heating the sample at the center (figure 2.2) [20]. Due to the large length to diameter ratio of test specimen

and use of end guard heater, the end effects are assumed negligible. The sample is then heated at constant power by applying alternating current in the line or cylindrical heater. When the steady state is reached, the temperatures at two radial positions are measured with the sensors located inside the sample. With known heating power, length of cylinder and measured temperature difference at two radial positions, the thermal conductivity of the sample is calculated using equation 2.3 which the simplified Fourier's equation for the radial heat conduction.

$$\dot{Q} = - \frac{2\pi \, k \, L \, (T_1 - T_2)}{\ln \, (r_2 / r_1)} \tag{2.3}$$

where: L = length of cylinder [m]

r_1, r_2 = radius of two location [m]

T_1, T_2 = temperature at two radial position [°C]

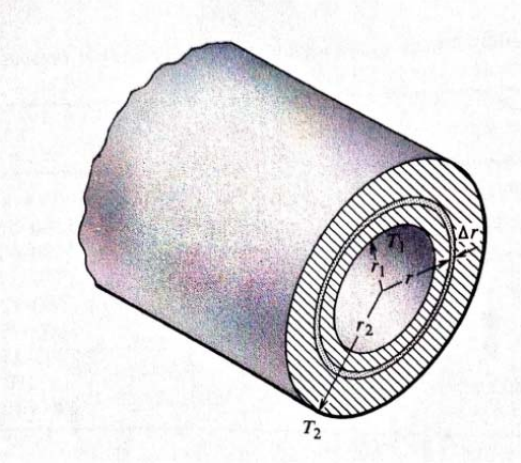

Figure 2.2 A schematic of cylindrical shell showing the elemental control volume for radial heat conduction.

This method of measuring the thermal conductivity is applied in this research with a slight modification in heating source. Instead of cylindrical electrical heater at the center of the sample a laser source has been used to heat the sample. The use of laser source reduces any complexity in fabrication of the heater on the surface of the thin film making the sample preparation and the experimental setup easier and simple.

2.2.3 3-ω Method

This method was originally proposed for measuring the thermal conductivity of isotropic bulk materials with low thermal conductivity and later it had been widely applied in measuring thermal conductivity of thin films deposited on high thermal conducting substrates. Corbino [37, 39] had measured a small third harmonic voltage component while applying alternating current to a heater which eventually originated the 3-omega method. Cahill [23, 37] popularized this method for measuring the thermal conductivity and specific heat of substrate materials and obtained an analytical solution for a vanishingly thin but finite width heater. This method employs thin metal strip on a substrate is used both as heater and as thermometer because its electrical resistance is dependent on temperature. When a sinusoidal current at frequency omega is passed through the metal strip, heating of underlying matter occurs at the second harmonics (2-omega) resulting a temperature fluctuation at 2 omega. Because the electrical resistance of the metal strip is dependent on the temperature, the temperature fluctuation leads to the change in the electrical resistance at 2 omega. Eventually

3-omega voltage is superimposed on the initial voltage due to the mixing of resistance and current sinusoids at different frequencies. This voltage at the third harmonic (3-omega) is then used to obtain useful information about the thermal properties of the system like the temperature oscillation.

Although this method has been widely used in measuring the thermal conductivity of thin films and substrate, there are certain limitations. The method employs formulas that are based on zero heater thickness and has to be long. It has been proved that the temperature oscillation would reduce at a lower frequency when finite length and thickness of heater is taken into account [37]. The fabrication of such heater on the surface of the thin film is again work of extreme complexity. Also the 3-omega voltage produced on the thin heater which is typically one thousand of the primary voltage is difficult to measure or is associated with amplification uncertainties. A schematic of traditional method of 3-omega used for measuring the thermal conductivity of the substrate is shown in figure 2.3 below [34].

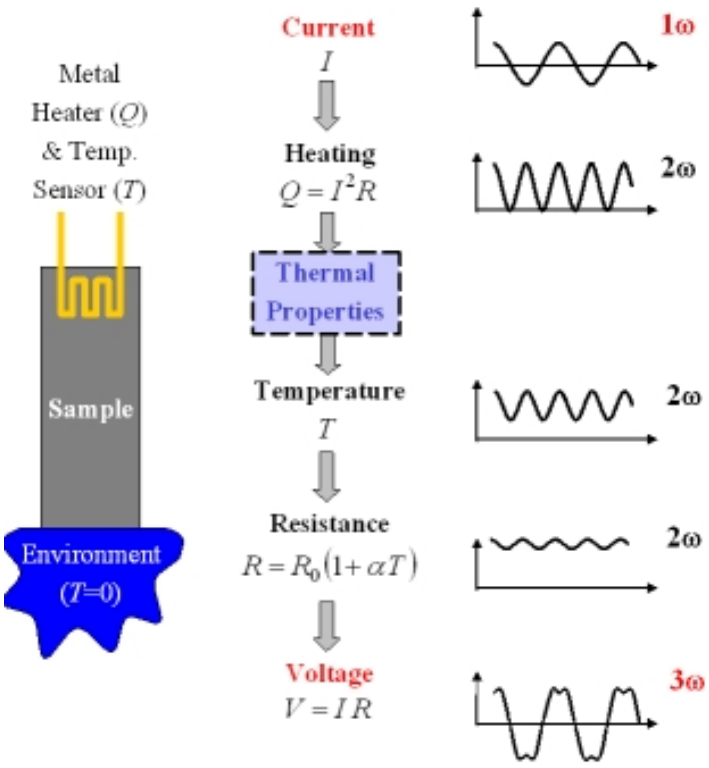

Figure 2.3 Three-omega method for thermal conductivity measurement.

2.3 Transient Methods

Transient method which includes thermal wave techniques (frequency domain) and pulse techniques (time domain) had been widely used to measure the thermal diffusivity of the thin film. This technique requires less precise alignment and dimensional knowledge and stability. The main advantage of this method over the steady state is the speed of the measurement as data can be recorded in short duration rather than a long wait to achieve a steady state measurement. However the measurement from this method is not as accurate as that of the steady state. In case of the thin film the accuracy of the measurement is of high priority as a slight deviation can result in misinterpretation of the

properties of the material. There are numerous types of transient methods but the thesis utilizes the steady state method and therefore one of the techniques which is most common and has greater applicability is discussed here.

2.3.1 Transient Hot Wire Technique

This method also known as a line heat source method is based on the thermal conduction due to a very thin linear heat source of infinite length. Its popularity is due to its wide application to measurements in material at all state, solids, liquids and gases. The line heat source is either embedded inside a solid sample or put in an enclosure such that fluid sample would surround the line heater [40]. Then a voltage is applied to produce a constant power and heat flux in the sample. The temperature response of the material with time is then evaluated from the change in resistance of the heating wire itself which is then related to the thermal conductivity of the material. The advantage of this technique over other transient methods is its simplicity of finding the thermal conductivity of the material directly from the slope of the line relating the temperature rise of the wire to the logarithm of time.

The temperature rise $\Delta T(r,t)$ at radial position r from the heat source when constant quantity of heat q per unit time and per unit length of the heating wire, initiated at the time t=0, produces the radial heat flow around the wire is given by the equation below.

$$\Delta T\left(r, t\right) = \frac{q}{4\pi\, k} \ln \frac{4\alpha\, t}{r^2 C} \tag{2.4}$$

where: $\triangle T(r,t)$ = temperature rise of wire at radius r at time t [°C]

q =heat production per unit time per unit length [W/m]

α = thermal diffusivity (m^2/s)

C = a known constant

The delicacy of the thin long heating wire that has to be used in this techniques and the difficulty in the sample preparation are some of the drawbacks which must have prevented the commercial development of devices utilizing this technique. Some of the commercially available devices based on the transient methods are Hot disk instrument, Heated needle probe and Laser flash instrument. However these devices are developed for measuring the thermal conductivity of bulk material and not useful in measuring properties in micro scale.

2.4 Thermocouple Based Method

A thermocouple is a junction between two different metals and is based on the principle that when the ends of two dissimilar metals joined together are maintained at different temperatures then voltage is generated across the ends (figure 2.4). This effect was discovered by Thomas Seebeck in 1821 and is known as Seebeck effect [33]. All types of dissimilar metals exhibit this effect [35]. The change in voltage with respect to a change in temperature is called Seebeck coefficient or thermoelectric sensitivity of the metal. This coefficient is usually a nonlinear function of temperature. However for a small change in temperature this coefficient is constant. Therefore the relationship between the

voltage difference generated by the two metals and the corresponding temperature gradient can be written in the linear form as

$$V_{AB} = S_{AB} \Delta T_s \quad (2.5)$$

where: ΔV_{AB} = Seebeck voltage [micro Volts]

S_{AB} = Seebeck coefficient [μV/°C]

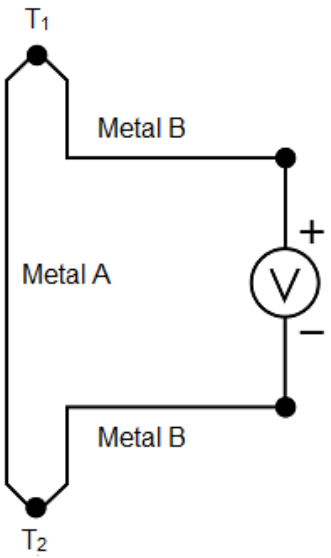

Figure 2.4 Schematic showing the seebeck effect.

Thermocouples are most commonly used temperature sensors as they are inexpensive and varieties of thermocouple are commercially available which can measure a wide range of temperature. The table 2.1 summarizes some of the common types of thermocouple with list of positive and negative electrode materials used for producing the thermocouple and its range of temperature measurement [31].

Table 2.1 Some common types of thermocouple commercially available.

Thermocouple Type	Materials used	Useful Application Range
B	Platinum30% Rhodium (+) Platinum 6% Rhodium (-)	2500 -3100 F 1370-1700 C
C	W5Re Tungsten 5% Rhenium (+) W26Re Tungsten 26% Rhenium (-)	3000-4200 F 1650-2315 C
E	Chromel (+) Constantan (-)	200-1650 F 95-900 C
J	Iron (+) Constantan (-)	200-1400 F 95-760 C
K	Chromel (+) Alumel (-)	200-2300 F 95-1260 C
N	Nicrosil (+) Nisil (-)	1200-2300 F 650-1260 C
R	Platinum 13% Rhodium (+) Platinum (-)	1600-2640 F 870-1450 C
S	Platinum 10% Rhodium (+) Platinum (-)	1800-2640 F 980-1450 C
T	Copper (+) Constantan (-)	-330-660 F -200-350 C

2.4.1 Thermocouple Circuit

Figure 2.5 below is the schematic of a typical thermocouple circuit. According to the seebeck effect a conductor subjected to a thermal gradient generates seebeck voltage. In order to measure this voltage a voltmeter has to be connected which involves connecting another conductor i.e., lead wires from the voltmeter. This additional lead wire will create extra junction and generate its own seebeck voltage that will oppose the original voltage. The magnitude of the effect depends on the seebeck coefficient of the different metals used.

In figure 2.5 metal A and metal B joined together creates a junction which is attached to the sample surface whose temperature T_{Tip} is to be measured. When voltmeter is connected in order to measure the seebeck voltage, two more junctions (reference junctions) are created. We intend to read the voltage generated across the thermocouple however this voltage is not generated at the junction of the two metals of the thermocouple but rather along that portion of the length of the two dissimilar metals that is subjected to a temperature gradient. Therefore two voltages equal and opposite are generated along metal A to Lead wire junction and then metal B to Lead wire junction when the reference junction is kept at a constant temperature, T_{Ref} with use of a isothermal block.

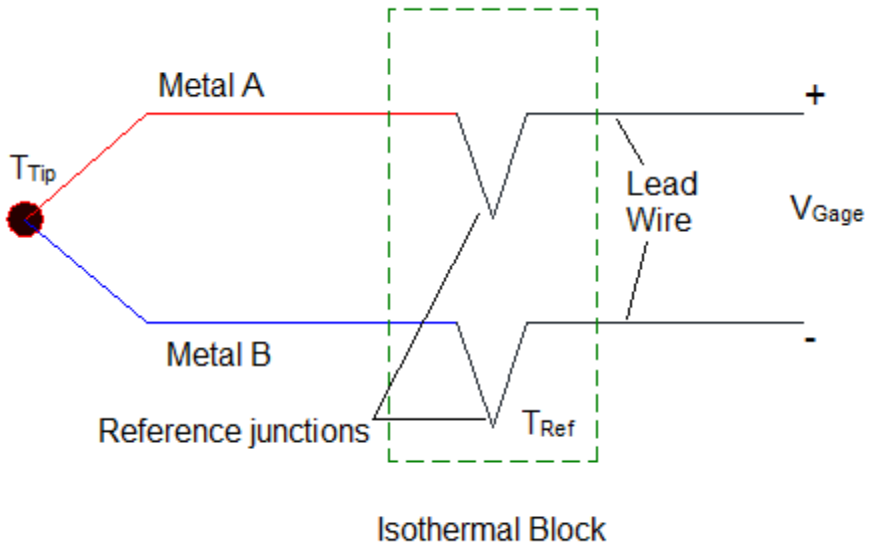

Figure 2.5 Schematic of thermocouple circuit.

Suppose the seebeck coefficient of metal A, metal B and lead wires are S_A, S_B , and S_{Lead} respectively These seebeck coefficients are temperature dependent Then the voltage output V_{Gage} measured by the voltmeter can be written as

$$V_{Gage} =$$

$$\int_{Gage}^{Ref} S_{Lead}\,(T)\frac{dT}{dx}dx + \int_{Ref}^{Tip} S_A\,(T)\frac{dT}{dx}dx + \int_{Tip}^{Ref} S_B\,(T)\frac{dT}{dx}dx + \int_{Ref}^{Gage} S_{Lead}\,(T)\frac{dT}{dx}dx$$

$$V_{Gage} = \int_{T_{Ref}}^{T_{Tip}} S_A\,(T)dT - \int_{T_{Ref}}^{T_{Tip}} S_B\,(T)dT$$

$$V_{Gage} = \int_{T_{Ref}}^{T_{Tip}} [S_A\,(T) - S_B\,(T)]dT \qquad 2.6$$

Within a small temperature range the seebeck coefficient is nearly constant for the metals and the combined seebeck coefficient can be calibrated

for that temperature range [33]. Suppose S_{AB} is the combined seebeck coefficient for the two metals then the integral in above equation can be reduced to relate the temperature at the tip of the thermocouple to the voltage readout by the following equation.

$$V_{Gage} = (S_A - S_B)(T_{Tip} - T_{Ref})$$

$$T_{Tip} = T_{Ref} + \frac{V_{Gage}}{S_{AB}} \qquad 2.7$$

From above equation it is clear that thermocouples can only measure temperature differences and a known reference temperature is required to yield the absolute readings.

2.4.2 Cold Junction Compensation

Thermocouples measure the temperature difference between two points, not absolute temperature. In order to measure the absolute temperature, the junction created by the connection by the lead wires to the thermocouple metals, known as cold junction has to be maintained at known reference temperature (see Fig 2.5). One way to accomplish this is to place the reference junction into an ice bath. Then from equation 2.7 the voltage readout can be directly employed to evaluate the absolute temperature of the sample. This is known as cold junction compensation.

However it is inconvenient to fix the ice bath temperature and is impractical outside the laboratory. In commercially available thermocouples, a separate temperature sensor such as thermistor is incorporated to provide the

temperature of reference junction. Some of the alternate methods used for the cold junction compensation are described below.

Electrical Bridge Method:

In this method a self compensating electrical bridge network as shown in figure 2.6 is incorporated to generate an equal and opposite voltage to cancel out any voltage introduced by the difference in the preset reference temperature at the cold junction and the surrounding [36]. A temperature sensitive resistance element such as thermistor is incorporated to measure the temperature of the cold junction. When the temperature of the surrounding changes, thermally generated voltage appears in the bridge, which is then energized from a stable dc power source to produce equal and opposite voltage in series to cancel the generated voltage. Thus the equivalent reference junction temperature is maintained over a wide ambient temperature range with a high degree of accuracy. For example integrated circuits such as the LT1025 are designed to output a compensated voltage based on thermocouple type and cold junction temperature.

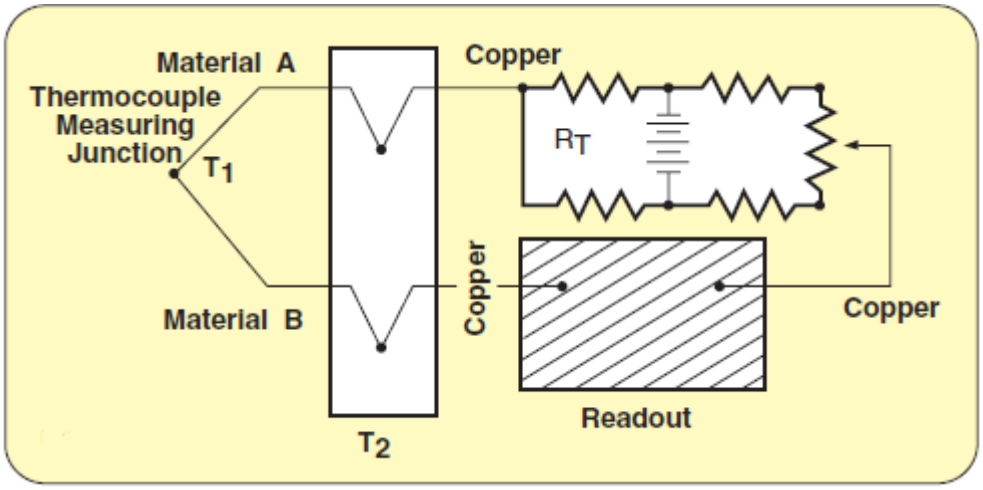

Figure 2 6 Thermo electric bridge method.

Thermoelectric Refrigeration Method:

This method is based on the ice bath compensation method. Thermoelectric ice point reference chamber (TRC), commercially produced by Omega technology, maintains reference junction at 0°C at atmospheric pressure. Pure distilled, de-ionized water inside a sealed cylindrical chamber is freezed by thermoelectric cooling elements mounted on the outer walls of the chamber [36]. This device is provided with sensors and micro-switches to automate the energizing and de-energizing of the cooling element to maintain the freezing temperature of the chamber. The schematic is shown in figure 2.7. Completely automatic operation eliminates the need for frequent attention required of common ice baths. The absolute temperature can be directly measured by the thermocouple without making corrections for reference junction temperature. Any type of thermocouples can be used with this instrument as the cold junction

compensation can be done with simple insertion of reference junction into the chambers.

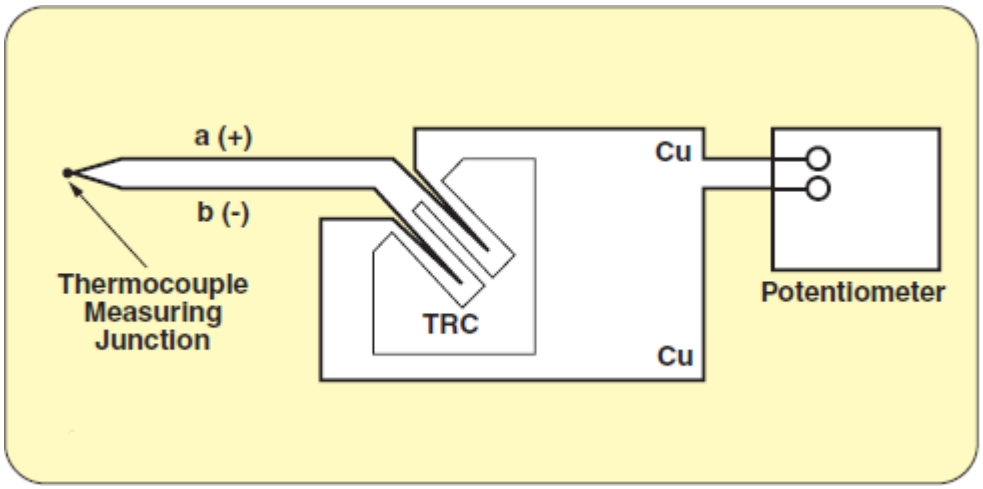

Figure 2.7 Schematic of thermoelectric refrigeration method.

Heated Oven Method

In this method two temperature-controlled ovens are used to simulate ice-point reference temperatures as shown in figure 2.8 [36]. Depending on the thermocouple type to be used two ovens are maintained at different temperatures such that the voltage generated by the reference junctions would be equivalent to the voltage produced during the junction kept at freezing point.

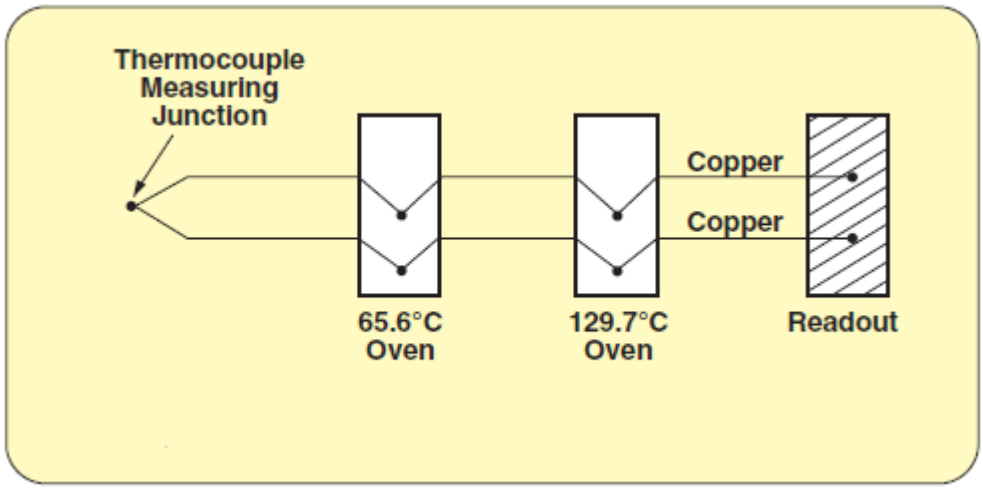

Figure 2.8 Schematic of heated oven method for cold junction compensation.

Although these are some of the commercially available cold junction compensation devices, an isothermal block prepared in the laboratory was used to maintain the reference junction at a constant temperature above the room temperature. This is detailed in Chapter 3.

2.5 Natural Convection

Natural convection is a mechanism in which the fluid motion is generated by buoyancy force due to density differences in the fluid occurring due to temperature gradients [20]. Whenever a fluid is heated or cooled there is a possibility of natural convection. Although one of the assumptions made in this thesis is that heat transfer in the thin film is a sole effect of heat conduction in one dimension, it is necessary to find out any potential heat loss due to the natural convection that might have a significant effect in the measurement of the

thermal conductivity. A literature study was therefore done to understand the phenomena of natural convection and determine the heat loss.

In a natural convection there is no characteristic velocity of the fluid and instead of Reynolds number, Grashof or Rayleigh number has the significant role in determining the fluid flow behavior. For a horizontal heated cylinder, according to Churchill and Chu [20] the flow is laminar if Rayleigh number falls in between values 10^{-6} and 10^{9}. The Rayleigh number is defined as

$$\mathrm{Ra_x} = \mathrm{Gr_x}\,\mathrm{Pr} \qquad 2.8$$

$$\mathrm{Gr_x} = \frac{\beta\,\Delta T\, g\, x^3}{\nu^2} \qquad 2.9$$

where: $\mathrm{Gr_x}$ = Grashof number

Pr = Prandtl number

β = volumetric coefficient of expansion [1/K]

g = gravitational acceleration [m/s^2]

ΔT = temperature difference between surface and fluid[K]

x = characteristic length [m]

α = thermal diffusivity [m^2/s]

ν = kinematic viscosity [m^2/s]

According to Lienhard [20], the average Nusselt number for an object of any arbitrary shape with laminar natural convection boundary layer is approximately related by

$$\overline{\mathrm{Nu_x}} = 0.52\ \mathrm{Ra_x^{1/4}} \qquad 2.10$$

where: x = characteristic length = D/2 for a cylinder [m]

D = diameter of cylinder [m]

After determining the Nusselt number from equation 2.10, the average heat transfer coefficient, $\overline{h_x}$ for the medium is estimated using

$$\overline{Nu_x} = \frac{\overline{h_x} D}{k} \qquad 2.11$$

Once the average heat transfer coefficient for the medium is known we can evaluate the heat lost due to the natural convection using Newton's law for cooling which is described by

$$\dot{Q} = h A (T_s - T_f) \qquad 2.12$$

where: h = convective heat transfer coefficient [W/m^2K]

A = surface area [m^2]

T_s = surface temperature of sample [K]

T_f = averaged fluid temperature [K]

CHAPTER 3

METHODOLOGY AND MATERIALS

In this chapter, the fabrication and calibration method of the micropipette thermal sensor employed for the thermal conductivity measurement will be outlined. This chapter also presents the description of experimental instruments, setup and procedure followed for the measurement of the thermal conductivity of the carbon nanotubes (CNT hereafter) film.

3.1 Micro-pipette Thermal Sensor

The thermal sensor used in this research is a thermocouple fabricated in the laboratory. The two metals used to create the thermocouple junction were Nickel (Ni hereafter) and lead free solder alloy which is basically alloy of Tin (Sn hereafter). The solder alloy used has a low melting temperature of approximately about 120^{o}C and therefore the sensors built in this research can be used to measure temperature rise below this temperature.

3.1.1 Fabrication of Pipette Sensor

To produce a sensing tip in micrometer size, a thick-wall borosilicate glass micropipette that is used in various biological applications for injecting biological solutions into tissues was used. A borosilicate glass tube with outer diameter of 1.5 mm and inner diameter of 0.86 mm was used for producing the micropipette.

The pipette puller (P-97, Sutter Instrument) was programmed according to the recipe to create patch pipettes with a tip size of 1 μm and approximately 5 to 7 mm long taper length (Fig. 3.1a).

The pulled pipette was filled with a lead-free soldering alloy mainly composed of Sn by an injection molding process in conjunction with localized heating of material. The injection molding was accomplished by mechanical pressurization (or pushing) of molten metal at the upper part of the pipette while heating the lower part near the tip with an electronic soldering gun maintained at 300 ^{o}C as shown in Fig. 3.1b.

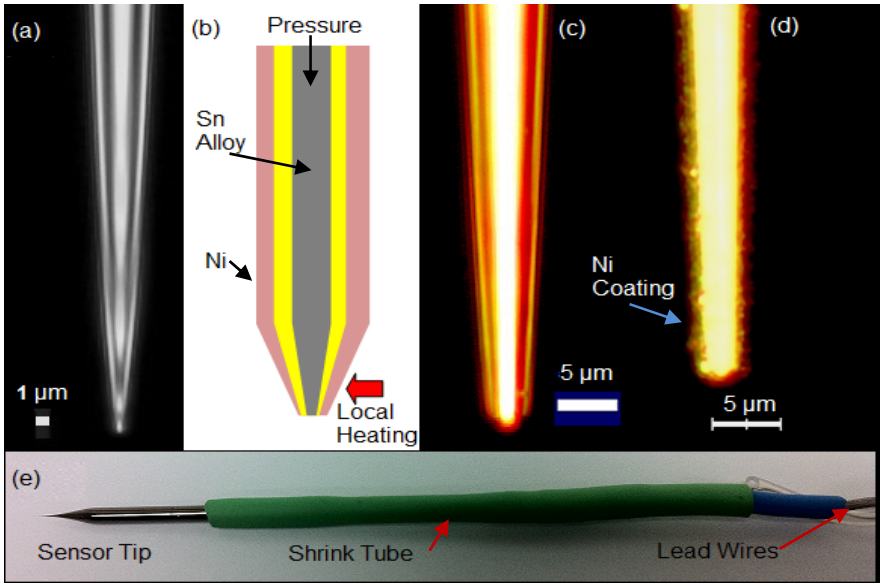

Figure 3.1 Fabrication steps of pipette thermal sensor: (a) an empty pipette with less than 1 μm opening; (b) a schematic outline of the filled pipette with a solder alloy and coated nickel; (c) after filling with a solder alloy and beveling; (d) after physical vapor deposition (PVD) thin film coating of nickel and silver; (e) a prototype micropipette thermal sensor.

The next step was beveling of the tip in order to remove unwanted metal extruded outside the pipette. This step is particularly important to assure there is a smooth and continuous contact between two metals after PVD sputtering of nickel. Therefore, BV-10 micropipette beveler (Sutter Instrument) that was designed for beveling micropipettes with tip diameters between 0.1 and 50 μm was used to sharpen and smoothen the tip. A 2-axis micromanipulator consisting of an angle plate to clamp the pipette was used to adjust the bevel angle between 25–30^{o}C. Controlled advancement of the pipette to an ultrafine grinding surface (with 0.3 μm alumina abrasive) was performed with use of coarse and fine control knobs mounted on the manipulator. The beveling process was monitored with a high magnification lens and a charge-couple device (CCD hereafter) camera (Mightex). The setup for beveling process is show in figure 3.2

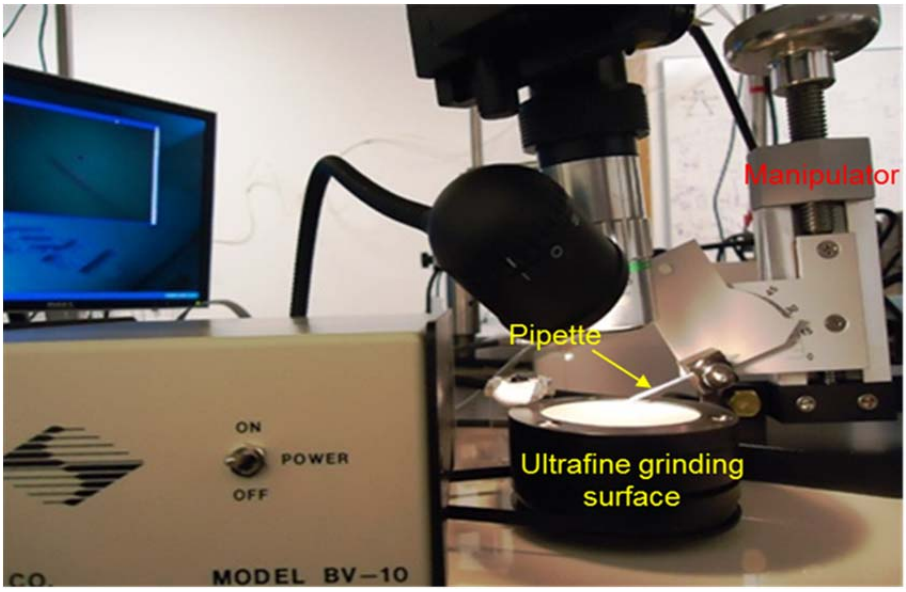

Figure 3.2 Image of the setup used for beveling of the micropipette with BV-10 micropipette beveler.

Image of the beveled pipette taken with Scanning electron microscope (SEM hereafter) as shown in Fig 3.3 revealed that the beveling process produced a smooth well leveled inclined glass and tin surface.

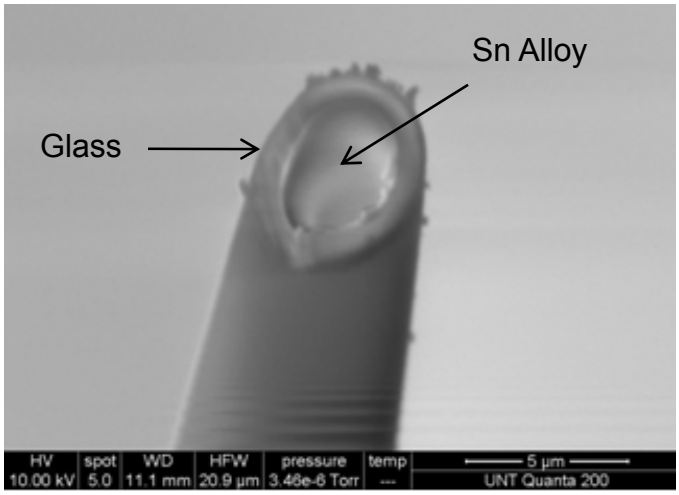

Figure 3.3 SEM image of beveled tip of micropipette prior to PVD deposition.

In order to investigate the effect of tip size on the thermoelectric power of the sensor, the pipettes were beveled to produce tip sizes varying from 2 to 30µm. Fig. 3.1c shows an image of a pipette, which was taken with a high-magnification optical microscope (Nikon Eclipse ME600) after beveling. The pipette was cleaned with ethyl alcohol using an ultrasonic cleaner (SHARPERTEK). Then a PVD technique [3, 4] was used to coat thin films of nickel on the outer surface of glass and thus forming a Ni-Sn alloy junction at the beveled tip (Fig. 3.1d). To analyze the effect on the sensitivity of the sensors due to the coating condition, batch of sensors were produced by differing the heating power to create the plasma of nickel target inside the PVD machine and also varying the deposition time. During the sputtering, the micropipettes were held at

vertical position facing directly opposite to the nickel target and rotated at a certain speed during the plasma creation and deposition so that uniform thin film of nickel would be created on the surface of the micropipette. Four batches of sensors were produced by varying the power from 200 to 300 W and deposition time from 30 minutes to 1 hour.

To connect the sensor with a voltmeter, lead wires (Sn alloy and Ni) were constructed at the end (opposite to the tip) of the micropipette by using the same material as the lead wires; this will prevent creation of unwanted signals from additional metal junctions unless otherwise compensated electronically. Therefore the Ni-wire was wound around the surface of the coated Ni and secured with epoxy. Similarly, the same solder wire, with ample length, was soldered to the inner Sn-metal at the end of the pipette. To strengthen the connection and minimize the contact resistance between the wound Ni-wire and the thin film Ni on the glass surface, a heat shrink tube was used on top of the junction (Fig. 3.1e).

3.1.2 Calibration

Calibration of the fabricated sensors was conducted in a thermally insulated calibration chamber filled with water. The calibration chamber was also fabricated in the laboratory whose schematic is provided in figure 3.4 and the picture of the chamber with insulation is shown if figure 3.5. The cylindrical body of the chamber was made of aluminum and the covering lid was made of Teflon.

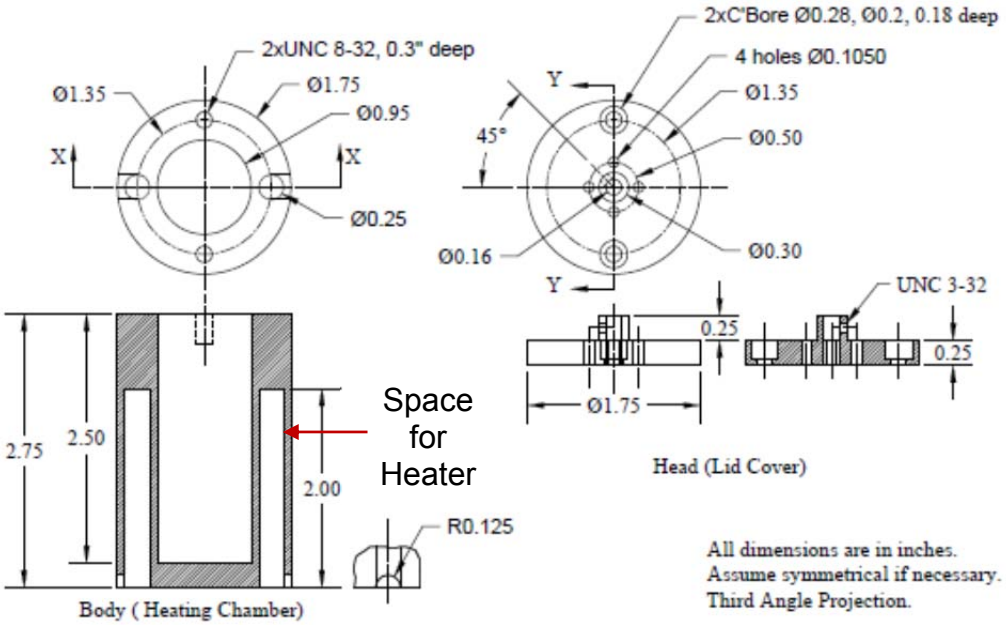

Figure 3.4 Schematic of calibration chamber.

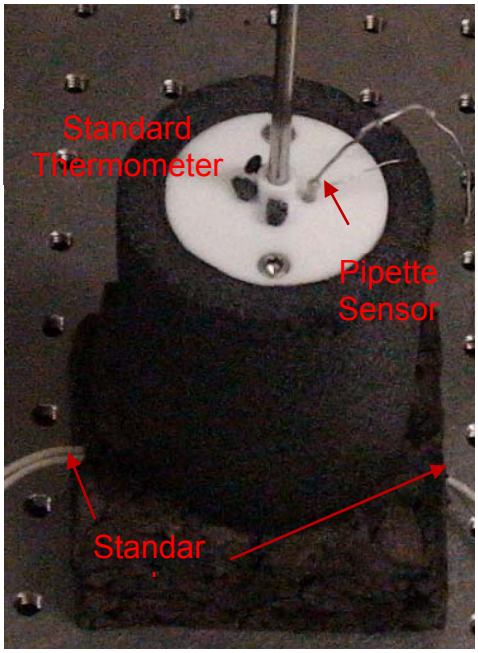

Figure 3.5 Image of the calibration chamber with insulation to maintain at a constant temperature.

The temperature of the water-filled chamber was controlled at a constant level with an accuracy of ± 0.1 ^{o}C. The temperature of the chamber was varied from room temperature of 21 ^{o}C to 40 ^{o}C by using an in-house temperature controller integrated with an automated data logging system with LabVIEW. A high-precision digital thermometer and the fabricated sensor were immersed into the water bath. Thus, both of them were in close proximity to indicate nearly the same temperature. The voltage generated by the sensor was recorded by a voltmeter (Nano Voltmeter, Keithley 2182). During the calibration process, the cold junction (Ni-Cu and Sn-Cu junction; a Cu lead wire from the voltmeter) of the sensor was maintained at a constant temperature (e.g. 24.5 ^{o}C) which was slightly above the room temperature using another lab built isothermal block made of aluminum so that unwanted additional thermocouple effects due to the cold junction could be removed. A plot of voltage signals provided by the sensor versus temperatures measured by a high-precision digital thermometer was obtained as shown in Fig. 3.6. The standard deviation in the voltage measurement was less than 0.018 μV which is equivalent to temperature rise of 0.002 ^{o}C.

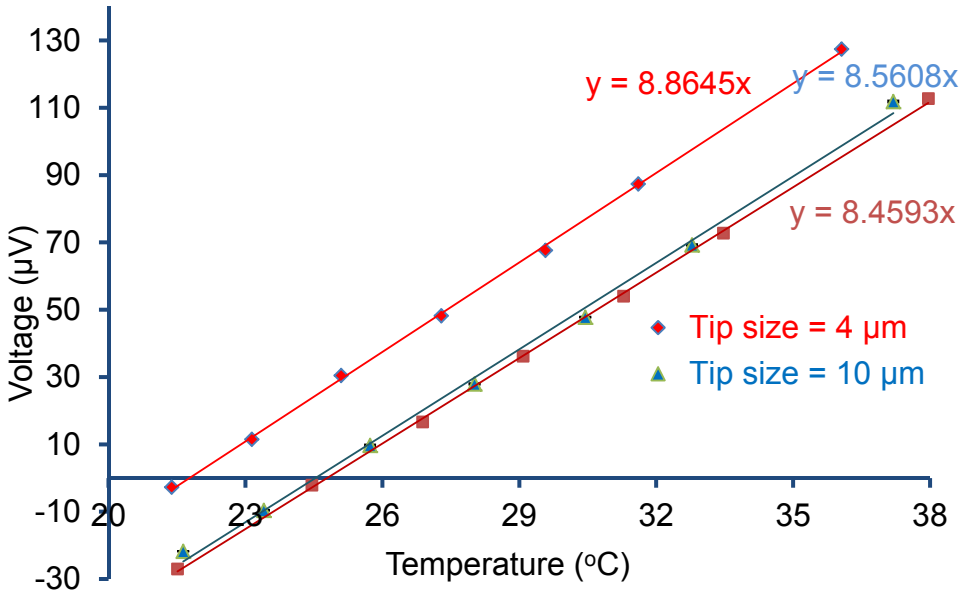

Figure 3.6 Calibration of sensors varying in tip diameters from 4 to 30 microns that were produced with the same PVD conditions.

Figure 3.6 depicts a linear relation between the recorded voltage and temperature increase. The thermoelectric power of the sensor can be obtained from the slope of the line in Fig. 3.6. Thus, fitting of the measured data with a linear trend line returned the slope (Seebeck coefficient) of 8.45, 8.56, and 8.86 μV/ ^{o}C for sensors with a tip size of 30, 10, and 4 μm, respectively.

3.2 Measurement of Thermal Conductivity of CNT Film

Two pipette sensors of approximately 3.5 μm sensing tip with seebeck coefficient of 5.67 and 7.44 μV/^{o}C were used to record the temperature difference at two positions on the surface of CNT film. The thin film of CNT on a polycarbonate substrate was prepared by the process discussed next.

3.2.1 CNT Film Preparation

CNT film was prepared by vacuum filtration. Vacuum filtration is a technique for separating a solid product from a solvent or liquid reaction mixture by suction created by vacuum underneath a filter. The device used for filtration mainly consists of a vacuum filter flask, a filter, a water pump and a Buchner funnel. The CNT film was prepared in the lab by following the procedures mentioned below.

1. The glass filter flask was first soaked with DI-water.
2. Nano-porous anodic aluminum oxide (AAO) membrane which serves as filter here to separate CNT from the solution was placed on top of the glass filter flask.
3. The membrane was then rinsed with deionized (DI) - water and vacuum was operated. With the AAO membrane being sucked down it was confirmed that vacuum was applied correctly and there were no leaks.
4. Then the Buchner glass-funnel was installed on top of it and secured to the position using aluminum clamp.
5. The glass funnel was then filled 2/3 with DI water.
6. CNT solution was poured in to the funnel and stirred to mix properly.
7. This vacuum filtration was allowed to run for some period.
8. When the water level in the funnel was about to reach half, DI water was added to fill up to initial level.
9. Step 8 was repeated for 2-3 times.

10. When all liquid was filtered, the AAO membrane containing the CNT film was removed carefully and allowed to dry in oven at 80 ^{o}C for 10-15 minutes.
11. Next sodium hydroxide (NaOH) solution was prepared in a Petri-dish and the membrane was immersed in the dish. Then 250 ml + 30 g NaOH solution was prepared and sonicated for 1 hour.
12. After sonicating process membrane was left in the solution for ½ hour and then all NaOH was removed with vacuum.
13. Then rinsing with DI water was repeated for 5 times.
14. In the last rinsing stage, desired substrate, here polycarbonate, was placed in the dish.

Finally the film was positioned on a substrate and dried in oven at 80 ^{o}C for half hour.

Figure below illustrates the steps 1 to 9 followed during the filtration process.

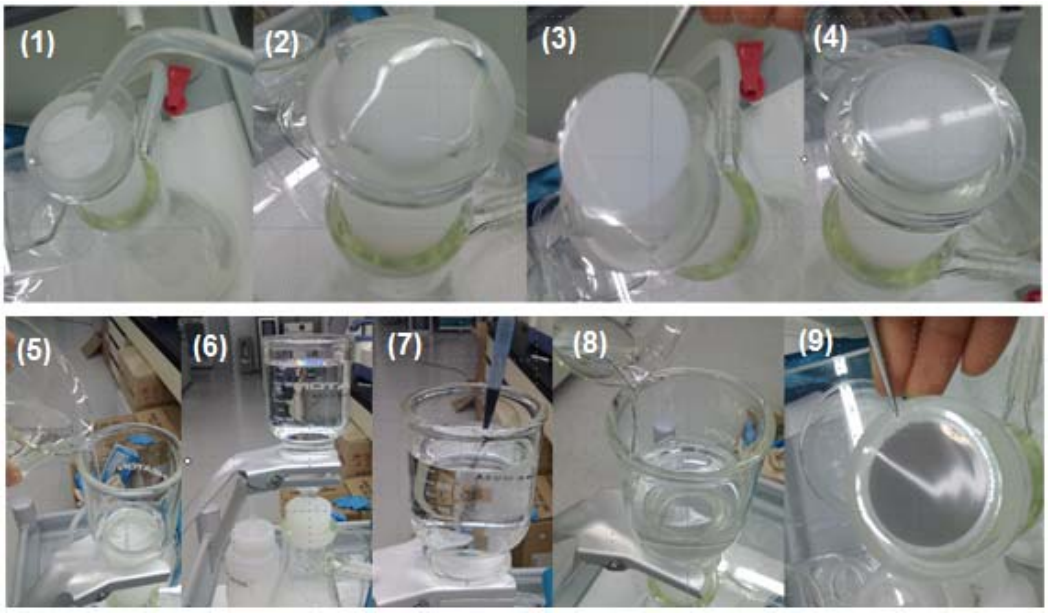

Figure 3.7 Steps in preparing CNT film on polycarbonate substrate.

Before the CNT film was prepared on the polycarbonate surface, number of holes, approximately 50 μm in diameter, were punched on the surface by laser drilling. The CNT film formed on these holes were therefore suspended from the polycarbonate. There is no contact in between CNT and polycarbonate substrate in this 50 μm diameter region. One of the CNT film in these holes were broken with a sharp tip of micropipette in order to measure the thickness of the film. SEM image as shown in figure 3.8 below demonstrated that the film was approximately 100 μm thick.

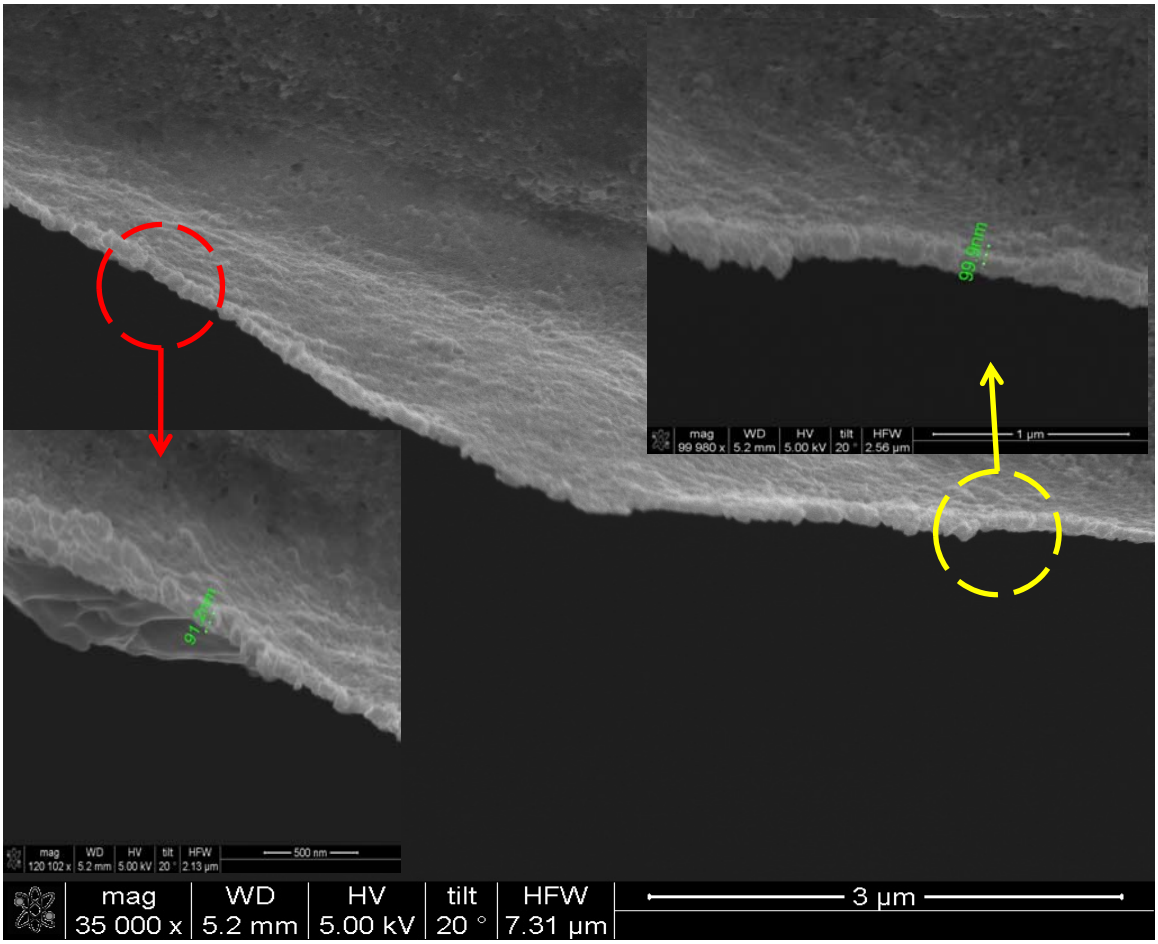

Figure 3.8 SEM image showing the thickness of the CNT film.

3.2.2 Experimental Setup

In order to measure the thermal conductivity of the CNT film developed on the polycarbonate surface a setup whose schematic is shown in figure 3.9 was prepared. A class B laser at 633 nm was irradiated at the center of the 50 µm cylindrical CNT film suspended on a polycarbonate substrate and the temperature difference at two radial positions were measured using the pipette thermal sensor.

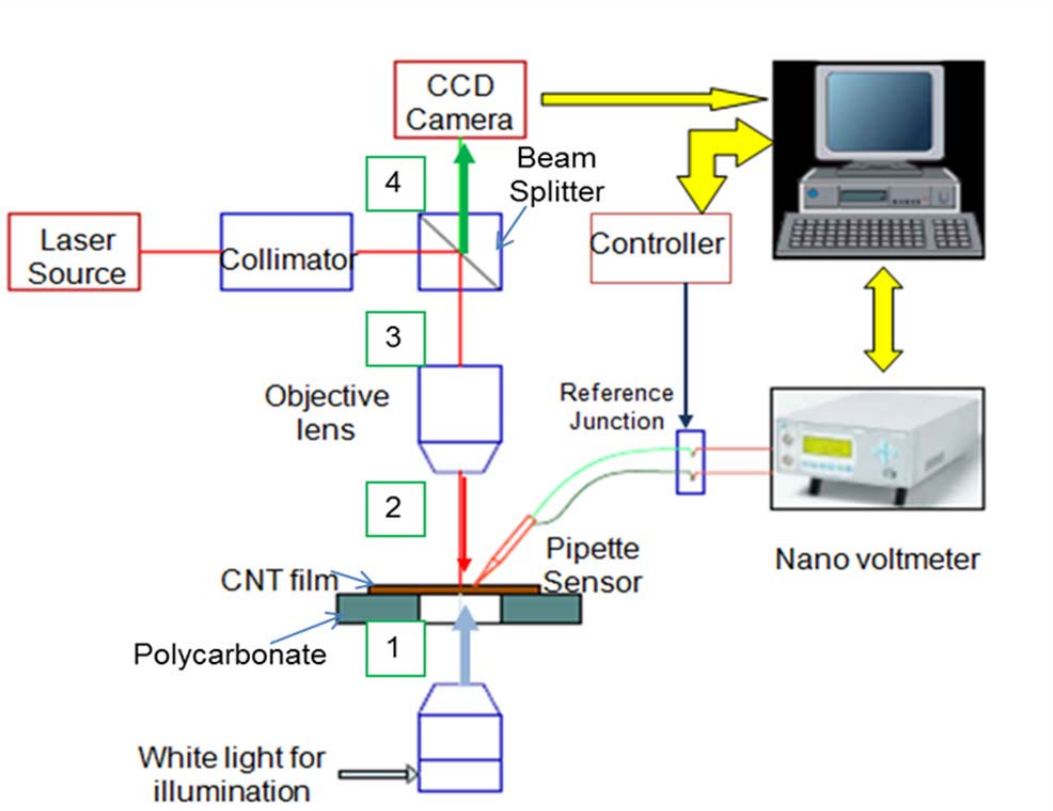

Figure 3.9 Experimental setup for the thermal conductivity measurement of CNT film with micropipette sensor.

Optical setup was prepared to guide the laser from the laser source positioned horizontally at a certain elevation from the surface of the working table. Combination of anti-reflection (AR) coated lenses from THORLABS were used to produce a collimated ray which was then diverted at 90^{o} by a beam splitter (THORLABS CM1-BS013) towards CNT film. A 20X objective lens (Mitutoyo MPlan Apo SL) was used to convert this diverted laser into a flat top laser of approximate diameter of 3 μm at the focal plane. White light from high intensity illuminator (Edmund optics MI-150) was guided with an optical fiber and

delivered through an objective lens to illuminate sample placed at the focal plane. The CNT film on the polycarbonate substrate was positioned horizontally in between two of the objective lens at the focal plane of 20X objective lens with use of XYZ motorized stage. In a similar approach, motorized stage was used to precisely control the movement of pipette sensor to position at a desired location on the surface of the thin film. Special care was taken to land the sensor on the CNT film as slight extra pressure would break the film.

A variable ND filter was used to control the power of the laser at a desired level. The film was placed at the focal point of the objective lens which was confirmed with the clear image obtained with the CCD camera as shown in figure 3.10(a). Laser was illuminated at the center of the film as shown in figure 3.10 (b) and then turned off momentarily to position the pipette sensor. Then the sensor was brought to a position (figure 3.10 c) such that its radial position r>6μm in order to avoid the direct laser shining at the tip of the sensor. Extensive care was taken while landing the pipette sensor on the film. Whenever a slight movement was recorded on the film by the CCD camera during the positioning of the sensor, the further movement of the sensor was stopped. In order to minimize the contact resistance in between sensor and film, a slight further movement to the sensor was provided by motorized controlled stage. At this position the maximum voltage signal was recorded by the voltmeter which confirmed that the sensor and the film were in good contact. For consistency in measurement, same

process was repeated to measure the voltage signal at different locations on the film.

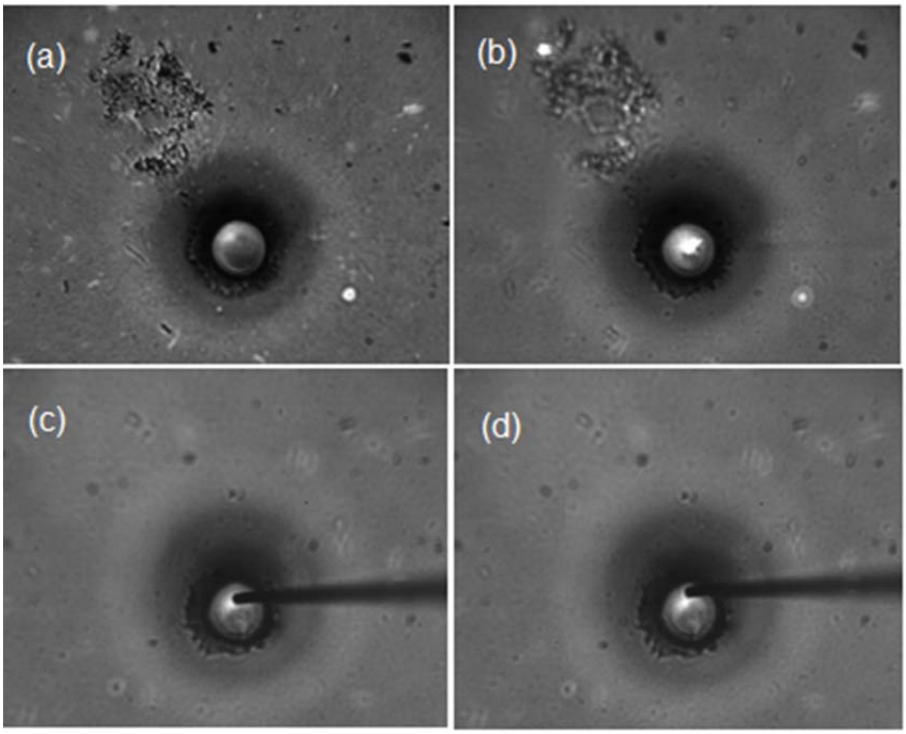

Figure 3.10 Measurement of temperature with pipette sensor. (a) CNT film at focal plane. (b) laser shined at the center of the film, (c) pipette sensor at position 1 and (d) pipette sensor at position 2.

Laser was then irradiated at a fixed power level (say 200 μW) and at the steady state the voltage generated by the sensor was recorded using nano voltmeter (Nano Voltmeter, Keithley 2182). The lab view program controlled the data recording such that voltmeter would record 3 data points returning their mean value every 10 seconds for 1 minute at the steady state (figure3. 11). The transmitted data to the computer was then recorded in a text file for post data

processing. It was observed that voltage signal was significantly higher when the laser was irradiating with sensor touching the film than when sensor was at the same position but not in contact with the film. This is the indication that the sensor is actually measuring the temperature rise due to heat conduction across the film.

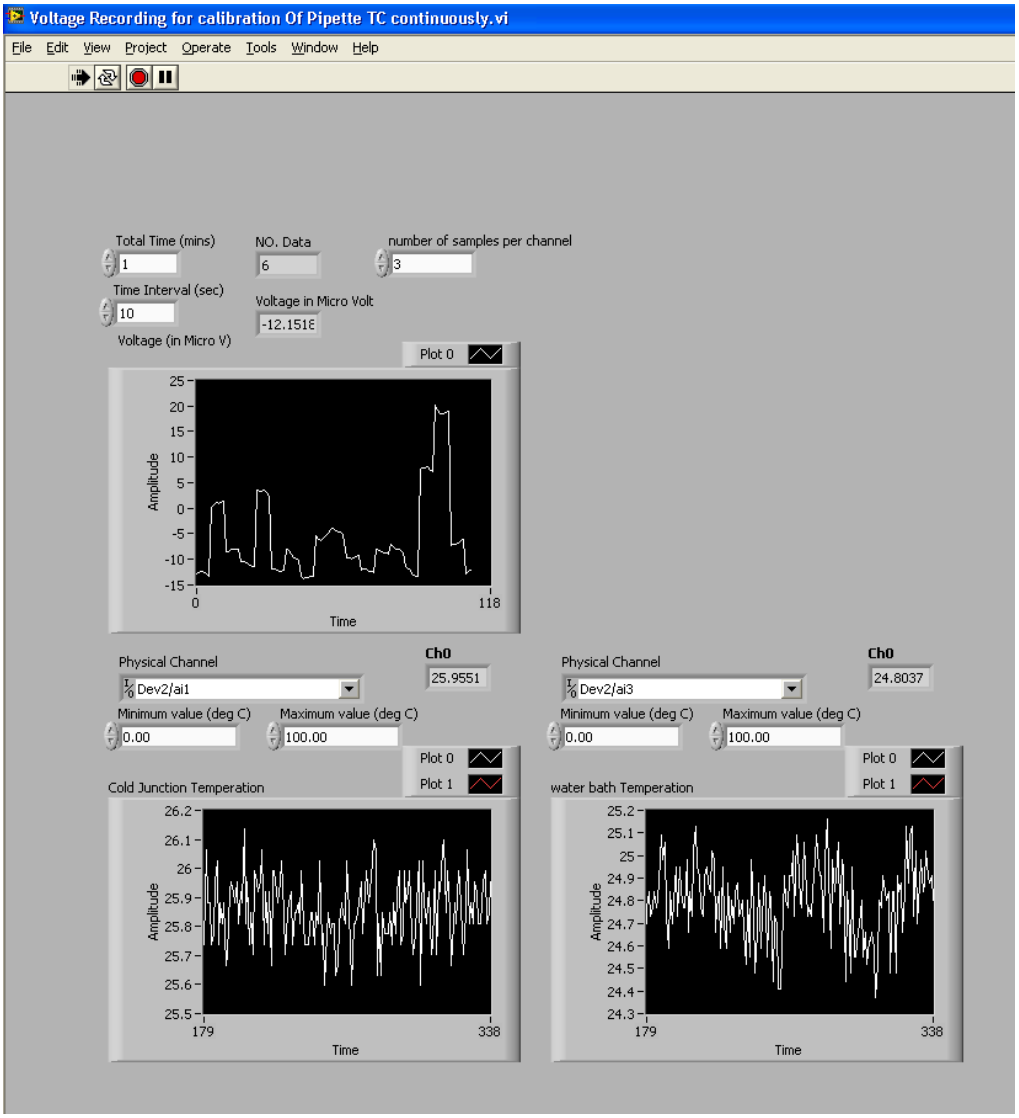

Figure 3.11 Lab view program used for controlling the voltage recording of the nano voltmeter.

The process was repeated to measure the voltage generated at location 2. With known seebeck coefficient of the sensor used, the voltages recorded at the two positions were then converted to temperature difference using equation 2.7. Figure below is the schematic of the model to demonstrate the radial heat conduction. It was measured and confirmed with the pipette sensor that the temperature at radius r> 25 μm was approximately close to room temperature.

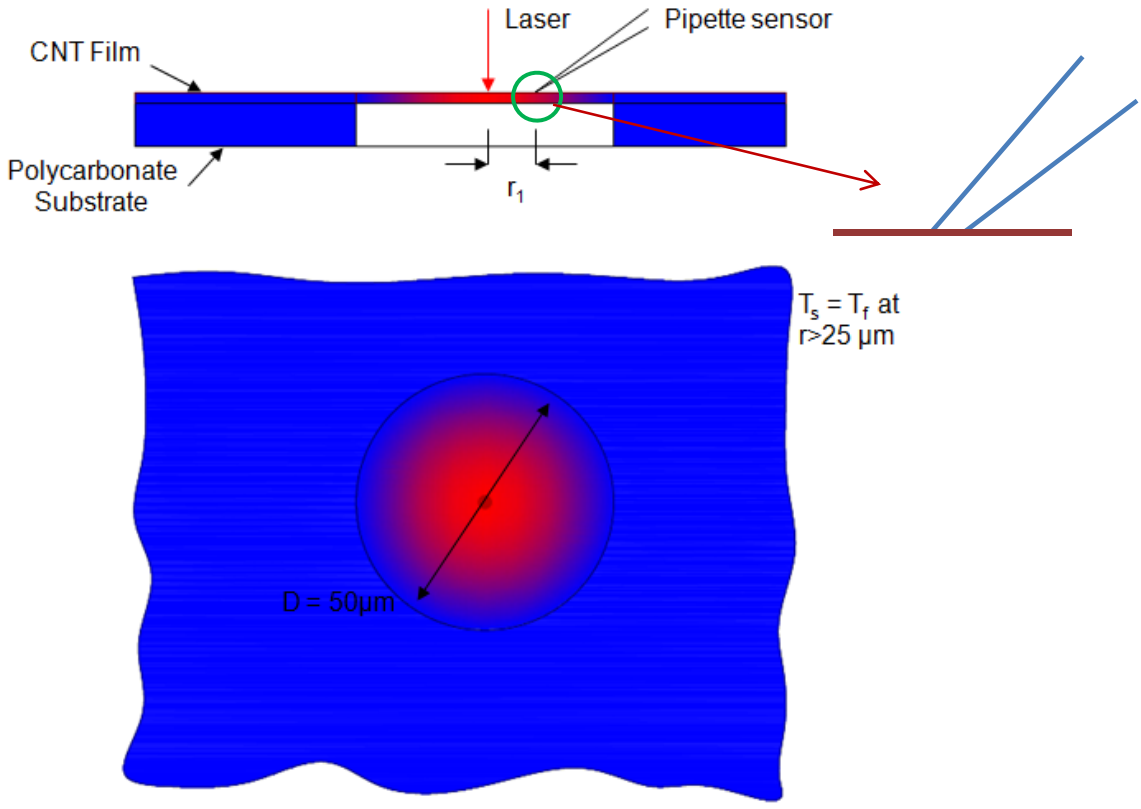

Figure 3.12 Schematic model showing the heat distribution in radial direction due to the laser shined at the center of the CNT film. It was measured and verified that for r> 25 μm surface temperature equals the temperature of surrounding.

The radial position of the sensor was determined by counting the pixel of the image taken by the CCD camera. The image taken from the CCD camera was first calibrated using the image taken with SEM.

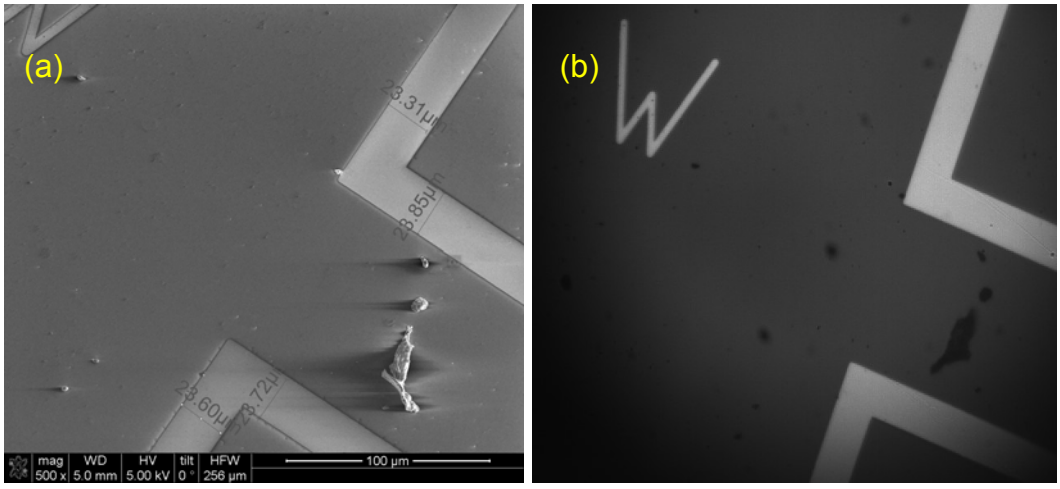

Figure 3.13 Calibration of image taken with CCD camera with SEM image (a) SEM image (b) CCD camera image.

3.2.3 Laser Power Measurement

Power absorbed during the laser irradiation at the center of the film is necessary to determine the thermal conductivity of the film. In order to determine the irradiated power absorbed by the film, conservation of energy was applied. This implies the amount of incident energy is equal to the sum of the absorbed, reflected, and transmitted energy.

Incident Energy = Absorbed Energy + Transmitted Energy + Reflected Energy 3.1

or, Absorptivity (A)+ Transmissivity (T)+ Reflectivity (R) =1 3.1 (a)

Digital Power meter (THORLABS PM100D) synchronized with the computer was used to record the laser irradiation power for 30 s at different positions 1, 2, 3 and 4 as shown in figure 3.9. Laser power measured at position 1 is the direct measure of the transmitted power whereas value at position 2 is the total incident power. Power measured at position 3 is used to determine the loss in the objective lens while power at position 4 is the reflected light taking into account all the losses in objective lens and beam splitter. From a separate measurement it was determined that the beam splitter refracts 45 % and reflects 55%. A mathematical relation relating the power at position 4 (P_4) with the reflected power (R) was developed as,

P_4 = [{R - (R x % loss in objective lens)}x 0.45] – [{R - (R x % loss in objective lens} x % loss in beam splitter] 3.2

Equation 3.2 can be used to determine the reflected power from the surface of the CNT film. Then with known power at position 1 i.e, transmitted power, absorbed power can be calculated using equation 3.1.

With a known absorbed power, radial positions and the temperature difference at two locations, thermal conductivity of the CNT film was calculated using equation 2.3 described in Chapter 2.

CHAPTER 4

RESULTS AND DISCUSSIONS

The first part of this chapter presents the results of the calibration of different pipette sensors produced by different physical vapor deposition (PVD hereafter) sputtering and the results of comparative study are discussed. Later we discuss the results of the measurement for the thermal conductivity of the carbon nanotubes (CNT hereafter) film.

4.1 Calibration of Pipette Sensor

The results of the calibrations of the pipette sensors are given in table 4.1. Four batches of thermal sensors were produced by varying the power and deposition time during PVD sputtering which are listed in the table. It was observed that the seebeck coefficient of the sensors produced by the same PVD condition were approximately the same and did not varied much for the different tip size. However, the increase in the deposition time and power i.e, deposition rate of the coating had significant effect on the seebeck coefficient of the sensors. Higher the deposition rate, higher was seebeck coefficient of the sensor.

All the sensors were calibrated at room temperature from 21 ^{o}C with an increment of 4 ^{o}C upto highest of 40 ^{o}C. The data obtained from the calibration were fitted with a linear trend line with R^2 value of 99% which provide the validation of equation 2.5 in Chapter 2 that indicated the linear relationship

between voltage and temperature. Therefore the seebeck coefficient of the sensor for this temperature range can be assumed to be constant and linear as well. Figure 4.1 to figure 4.4 are the plots of voltage versus temperature for different sensors produced with same PVD condition.

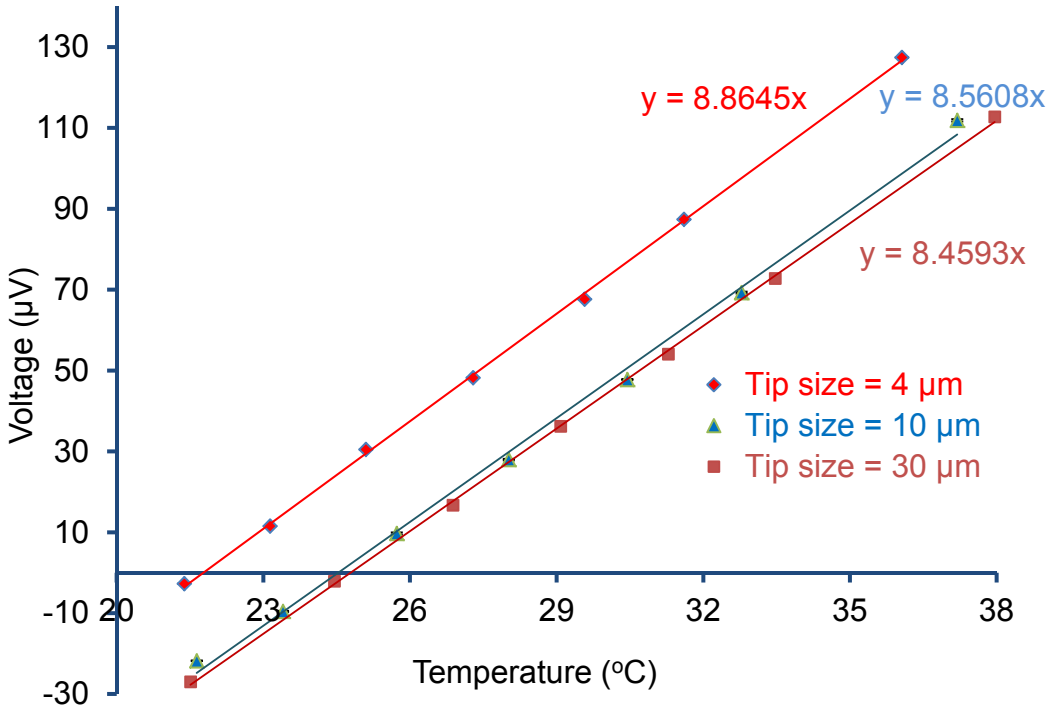

Figure 4.1 Calibration of sensors varying in tip diameters from 4 to 30 microns that were produced with the same PVD conditions (Power = 300 W, Deposition time = 1 hr).

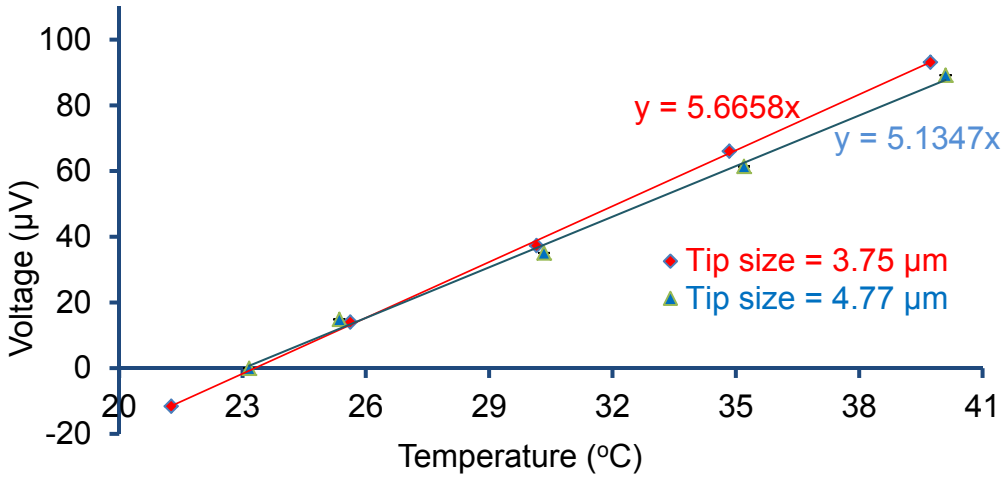

Figure 4.2 Calibration of sensors varying in tip diameters from 3.75 to 4.77 microns that were produced with the same PVD conditions (Power = 250 W, Deposition time = 45 mins).

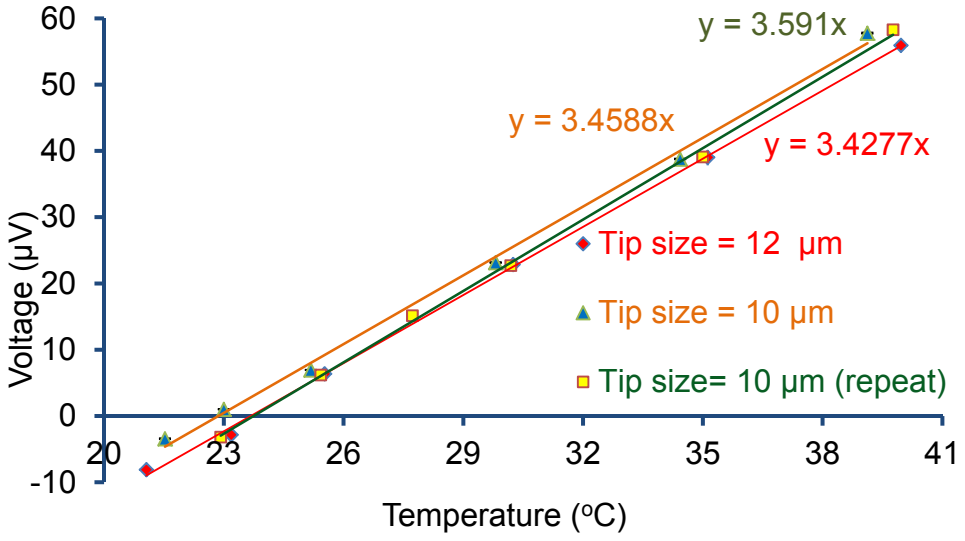

Figure 4.3 Calibration of sensors varying in tip diameters from 10 to 12 microns that were produced with the same PVD conditions (Power = 200 W, Deposition time = 30 mins).

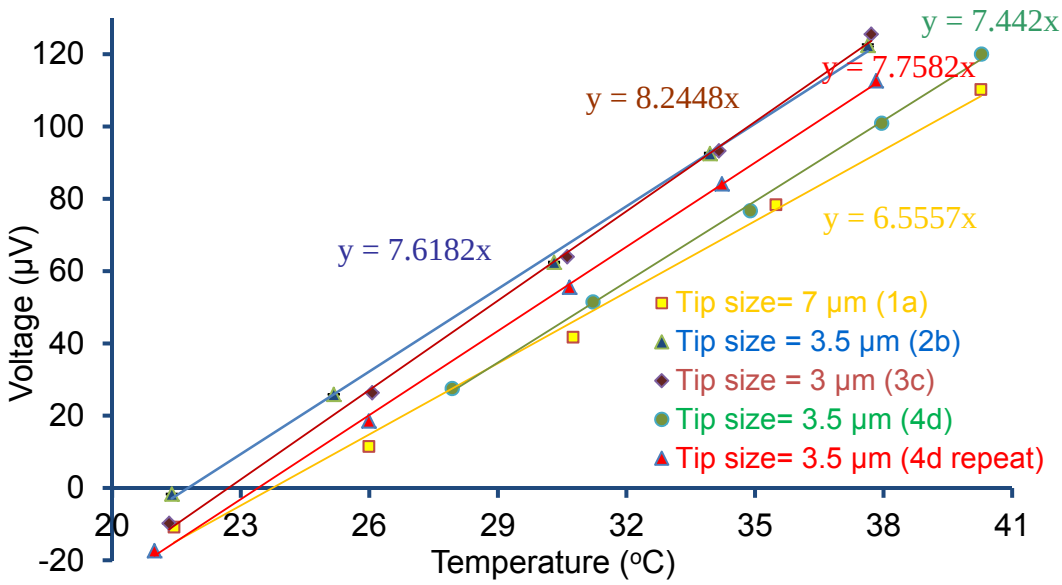

Figure 4.4 Calibration of sensors varying in tip diameters from 3 to 7 microns that were produced with the same PVD conditions (Power = 250 W, Deposition time=1 hr).

The calibration was repeated for some of the sensors to check the repeatability in measurement by the sensor. It showed that variation in seebeck coefficient was within 4%. This is an acceptable value as the error can be generated in the voltage measurement by voltmeter whose error in measurement was designated as ±0.02 µV. Also the instrumental error for the digital thermometer was same i.e, ±0.02 µV. Root Sum Square (RSS hereafter) method [38] was used to determine the uncertainty in the value of the seebeck coefficient determined by equation 2.5. This error was calculated to be ±0.05 µV/^{o}C for a unit change in voltage and temperature. During the measurement of voltage, a sensor with seebeck coefficient of 6.55 µV/^{o}C was capable of recording the data

with standard deviation of 0.01 which is equivalent to 0.002 ^{o}C change in temperature. Therefore the resolution of the sensor was determined as 0.002 ^{o}C.

Table 4.1 Seebeck coefficients obtained from the calibration.

PVD Coating Condition	Sensor Designation	Seebeck Coefficient (μV/ ^{o}C)	Tip Size (μm)
Power = 300W Depositon Time = 1hr	1	8.45	30
	2	8.56	10
	3	8.86	4
Power = 250W Depositon Time = 45 mins	4	5.14	3.75
	5	5.67	4.77
Power = 200W Depositon Time = 30 mins	6	3.46	10
	6 (repeat)	3.59	10
	7	3.43	12
Power = 250W Depositon Time = 1hr	1 (a)	6.56	7
	2 (b)	7.62	3.5
	3 (c)	8.25	3
	4 (d)	7.44	3.5
	4 (d) (repeat)	7.75	3.5

However the seebeck coefficients of the sensors are far below than those of bulk material, the possible cause of which can be related to the thermoelectric behavior of vapor deposited thin metal film. Hill et al. [7] explained the

dependency of thermoelectric power of a thin film using a conduction mechanism of free electrons in crystal lattice:

$$S = \frac{\pi^2 K^2 T}{3e\varsigma}\left\{\frac{d\ln\lambda(E)}{d\ln(E)}\right\}_{E=\varsigma} \qquad 4.1$$

where S = thermoelectric power,

K = Boltzmann constant,

e = electronic charge,

T = temperature (K),

ζ = Fermi energy,

λ = mean free path of the conduction electron, and

E = electron energy.

Here S is a function of Fermi energy and Mean free path (MFP), both of which are dependent on addition of impurities and the thickness of the film. A thickness of 80-90 nm is estimated based on the measurement of film thickness on a quartz substrate using a profile-meter after deposition. At this thickness, there is a possibility of formation of a large number of broad empty channels [11] incorporated with impurities and structural defects. This results in reduction of the mean free path and enhancement of the electrical resistivity, which explains the reduced seebeck coefficient in thin films well.

4.2 Thermal Conductivity Measurement of CNT Film

The results obtained for the thermal conductivity measurement of the CNT film is presented in table 4.2. Two pipette sensors with approximately same tip

size of around 3.5 μm but differing in the sensitivity i.e., seebeck coefficient were used to measure the temperature difference at two locations. From the result of the calibration of the sensors it was verified that the sensitivity of the sensor is dependent on the coating conditions. Higher the deposition rate, thicker the film of nickel will be formed at the tip of solder alloy filled micropipette creating the smooth thermocouple junction and producing the sensor with higher sensitivity. As the CNT film diameter was confined to 50 μm, there was a necessity to use the smallest tip pipette sensor to measure the temperature precisely within a limited region.

Experiment was carried out by irradiating laser at two power levels. Variable Neutral Density (ND) filter was used to fix the laser power at approximately 200 μW. Voltage at two different locations, approximately 8 μm apart in radial directions, were measured with sensor designated as Senor# 4d. Laser power at four location as discussed in section 3.2.3 were measured with the power meter in order to determine the power absorbed by the CNT film. Using equation 3.1 and with all the powers measured at the four locations, the power absorbed by the CNT film was determined as 65.60 μW which was about 75% of the total irradiated power. The radial position of the two locations was determined by counting the pixels in between the locations and center of the CNT film. The picture taken with charge-couple device (CCD hereafter) camera was calibrated with respect to scanning electron microscope (SEM) image and it was determined that 1 pixel in the image from CCD camera is equivalent to 0.5

μm. Then using equation 2.3 the thermal conductivity was determined as 75.004W/m^{o}C. The experiment was repeated at the same power level using the same pipette sensor but this time the temperature difference was measured for 2 new locations. The thermal conductivity of the film was calculated as 76.37 W/m^{o}C. Two more experiments were conducted with the same sensor with slight increment in laser power to approximately 250 μW. Obviously the value of the power absorbed increased to 79.2 μW but the percentage power absorption by the film remain approximately the same. The thermal conductivity of CNT with this experiment was calculated as 73.48 W/m^{o}C. Similar experiment was completed using pipette sensor with slightly smaller sensitivity. From the measurement the thermal conductivity was determined to be approximately 72W/m^{o}C. The thermal conductivity of the CNT film determined by two different sensors while differing the power level to irradiate the film were approximately the same value and therefore average value 73.418 W/m^{o}C was accepted as the thermal conductivity of the film. From the measurement the standard deviation in the thermal conductivity values is only 1.94 W/m^{o}C which is 2.64% error in the measurement.

To confirm that the heat transfer in the film was mostly due to the radial heat conduction in the film, the natural convection and radiation heat loss was also evaluated. When the laser was fixed at 250 μW (highest power used during the experiment), the sensor detected that the laser would produce a temperature of 27^{o}C at the center of the film. Since the experiment was conducted at a room

temperature of 21^{o}C, the mean film temperature to calculate the convection heat transfer was accepted as 24^{o}C. At this mean film temperature Rayleigh number was determined by using equation 2.8 and 2.9 as 2.79 X 10 $^{-4}$ which confirmed that there will be natural convection. Using equation 2.10, and 2.11 the convective heat transfer coefficient at mean film temperature of 24^{o}C for air was determined to be 22.85 W/m^{2} K. Then using equation 2.12 the heat loss due to the natural convection was determined to be 0.269 μW which is only 0.36 % of the absorbed power 73 μW (absorbed power assumed as average of the maximum and minimum power recorded during the experiment). Similarly using Stefan Boltzmann law, the heat loss to the surrounding from the film surface was calculated as 0.069 μW which is only 0.09% of the total power absorbed in the film. Therefore the heat transfer by natural convection and radiation was ignored and the temperature difference measured by the sensor was confirmed as the sole effect of the radial heat conduction in the film.

Table 4.2 Summary of the measurement to determine the thermal conductivity of CNT film.

Sensor no.	Tip Size (μm)	Seebeck Coeff. (μV/ ^{o}C)	Laser Power at origin (μW)	Power absorbed on CNT (μW)	r_1 (μm)	r_2 (μm)	Temperature Difference ($\triangle$T)	K (W/m.^{o}C)	Mean (W/m.^{o}C)	STD	% error
4d	3.50	7.44	217.17	65.60	8.48	16.43	0.920	75.004	73.418	1.940	2.643
			217.17	65.60	8.09	15.81	0.916	76.370			
			256.81	79.20	12.73	21.36	0.888	73.481			
			256.81	79.20	8.09	17.09	1.302	72.424			
5	3.71	5.67	234.00	66.50	6.70	11.07	0.743	71.384			
			254.55	82.21	6.97	13.94	1.262	71.847			

CHAPTER 5

CONCLUSIONS AND RECOMMENDATIONS

5.1 Conclusions

A novel technique for fabricating high-resolution micropipette thermal sensors using inexpensive materials was described. The developed technique can be implemented relatively easily in a laboratory setting. The micropipette sensors were manufactured by filling tin (Sn)-based alloy inside a glass micropipette and coating thin films on the outer surface of a glass micropipette by physical vapor deposition (PVD hereafter) so that a thermocouple junction was created only at the tip of micropipette. With a comparative study of the sensors produced by different PVD coating conditions, it was demonstrated that higher deposition rate would produce sensors with higher sensitivity and the sensitivity of the sensor would not be affected by the tip size. Sensitivity of the sensor was found as low as 3.43 μV/ ^{o}C and maximum of 8.86 μV/^{o}C depending on the coating conditions used for the fabrication. In this research, it was found that PVD coating with power at 300 W and deposition time of 1 hr would produce the sensors with maximum sensitivity. Calibration results show that the sensor is capable of measuring a temperature fluctuation of 0.002^{o}C.

Validity of the fabricated micropipette sensors was checked by measuring temperature at two locations on the surface of carbon nanotubes (CNT hereafter) film to determine its thermal conductivity. Temperature difference of

approximately 1 to 1.3 ^{o}C was recorded at two locations that were about 8 μm apart in radial direction. The heat loss by natural convection and radiation from the CNT surface to the surrounding was determined to be 0.36% and 0.09% respectively and therefore the temperature gradient at two locations was concluded as a sole effect of radial heat conduction on CNT film. When laser was irradiated at the center of the CNT film, 70 to 75% of power was found to be absorbed by the CNT film. Measurement performed by two different sensors with different sensitivity produced similar data results for same laser power. The calculated thermal conductivity of the CNT film using the measurement data varied from 71.384 to 76.37 W/m^{o}C. Although the measurements were performed with 2 different sensors with different laser irradiating power, the standard deviation in the calculated value for thermal conductivity was only 1.94 W/m^{o}C which is 2.64 percent of the mean value. Therefore the mean value 73.418 W/m^{o}C was accepted as the thermal conductivity of the CNT film at room temperature.

5.2 Recommendations

The following are a list for the possible future work that can be done in this study.

- Effect of the thickness of the Nickel coating on the seebeck coefficient of the sensor should be studied.

- In the fabrication of the sensor, the manual method of pressurizing the molten solder metal out of the pipette should be replaced by mechanical method so that tip size smaller than 1 μm can be produced.
- Nickel (Ni) is not a biocompatible metal therefore a protective biocompatible layer should be coated outside the Ni-coating in order to make these sensors useful in measuring the thermal properties of biological fluids at cellular level.
- Future work will involve use of the sensors in measuring thermal properties of biological fluids at a cellular level.

REFERENCES

[1] A. Helmy, M. Holdmann and M. Rizkalla, 2008. Application of thermography for non-invasive diagnosis of thyroid gland disease, IEEE transactions on biomedical engineering 55, 1168-1175.

[2] A. Majumdar, 1999. Scanning thermal microscopy, Annu. Rev. Mater. Sci. 29, 505-585.

[3] A. Mubarak, E. Hamzah and M. R. M. Toft, 2005. Review of physical vapour deposition (PVD) techniques for hard coating, Jurnal Mekanikal 20, 42-51.

[4] B. Navinsek, P. Panjan and I. Milosev, 1999. PVD coatings as an environmentally clean alternative to electroplating and electroless processes, Surface and Coatings Technology 116-119, 476-487.

[5] C. C. Wu and F. B. Wu, 2009. Microstructure and mechanical properties of magnetron co-sputtered Ni–Al coatings, Surface & Coatings Technology 204, 854–859.

[6] D. E. Blask, L. A. Sauer, R. T. Dauchy, E. W. Holowachuk, M. S. Ruuhoff and H. S. Kopff, 1999. Melatonin inhibition of cancer growth in vivo involves supression of tumor fatty acid metabolism via melatonin receptor-mediated signal transduction events, Cancer Research 59, 4693-4701.

[7] D. E. Hill, L. Williams, G. Mah and W. L. Bradley, 1997. The effect of physical vapor deposition parameters on the thermoelectric power of thin film Molybdenum-Nickel junctions, Thin solid films 40, 263-270

[8] G. Fish, O. Bouevitch, S. Kokotov, K. Lieberman, D. Palanker, I. Turovets, and A. Lewis, 1995. Ultrafast response micropipette- based submicrometer thermocouple, Rev Sci. Instrum. 66 (5), 3300-3306.

[9] G. V. Gavriloaia, A. Hurduc, A.-M. Ghimigean and R. Fumarel, 2009. Spatial-temperature high resolution map for early cancer diagnosis, SPIE 7171.

[10] J. Che, T. Cagin, and W. A. Goddard III, 1999. Thermal Conductivity of carbon nanotubes, The Seventh Foresight Conference on Molecular Nanotechnology. Santa Clara, CA.

[11] M. Adamov, B. Perovic and T. Nenadovic, 1974. Electrical and structural properties of thin gold films obtained by vacuum evaporation and sputtering, Thin Solid Films 24, 89-100.

[12] M. Mandel, L. Igambi, J. Bergendahl,M. L. Dodson, JR., and E. Scheltgen, 1970. Correlation of melting temperature and cesium chloride buoyant density of bacterial deoxyribonucleic acid, Journal of Bacteriology 101(2), 333-338.

[13] M. S. Watanabe, N. Kakuta, K. Mabuchi and Y. Yamada, 2005. Micro-thermocouple probe for measurement of cellular thermal responses, Proc. 27th Ann. Conf. 2005 IEEE EMB., 4858-4861.

[14] N. Kakuta, T. Suzuki, T. Saito, H. Nishimura and K. Mabuchi, 2001. Measurement of microscale bio-thermal responses by means of micro-thermocouple probe, EMBS International Conference. Istanbul, Turkey: IEEE, 3114-3117.

[15] R. H. Garrett and C. M. Grisham, 2007. Biochemistry updated third edition. Belmont, CA: Thomson Brooks/Cole.

[16] S. Kim, K. C. Kim and K. D. Kihm, 2007. Near-field thermometry sensor based on the thermal resonance of a microcantilever in aqueous medium, Sensors 7, 3156-3165.

[17] S. R. Choi and D. Kim, 2007. Measurement of Thermal Properties of Microfluidic Samples Using Laser Point Heating Thermometry, Thermochimica Acta 455, 11-15.

[18] U. F. Wischnath, J. Welker, M. Munzel and A. Kittel, 2008. The near-field scanning thermal microscope, Review of Scientific Instruments 79, 073708.

[19] W. Wu, J. S., P. Banerjee and S. Zhou, 2010. Core-shell hybrid nanogels for integration of optical temperatur-sensing, targeted tumor cell imaging, and combined chemo-photothermal treatment, Biomaterials, in press, doi: 10.1016/j.biomaterials.2010.06.030.

[20] A. F. Mills, 1995. Heat and Mass Transfer. California: Library of Congress Cataloging-in-Publication Data.

[21] A. Sohrabi, A. Dolati, M. Ghorbani, A. Monfared, and P. Stroeve, 2010. Nanomechanical properties of functionally graded composite coatings: Electrodeposited nickel dispersions containing silicon micro- and nanoparticles. Materials Chemistry and Physics 121, 497–505.

[22] C. Hu and S. Hu, 2009. Carbon Nanotube-Based Electrochemical Sensors: Principles and Applications in Biomedical Systems. Journal of Sensors.

[23] D. G. Cahill, R. O. Pohl, 1987. Thermal conductivity of amorphous solids above the plateau. Phys. Rev. B 35 (8), 4067-4073.

[24] D. Saraev, R. E. Miller, 2006. Atomic-scale simulations of nanoindentation-induced plasticity. Acta Materialia, 33-45.

[25] E. A. Pavlatou, M. Stroumbouli, P. Gyftou and N. Spyrellis, 2006. Hardening effect induced by incorporation of SiC particles in nickel electrodeposits. Journal of Applied Electrochemistry 36, 385–394.

[26] E. P. Sakonidou, H. R. van den Berg, C. A. ten Seldam and J. V. Senger 1999. An Improved Guarded Parallel-Plate Method for Measuring the Thermal Conductivity of Fluids in the Critical Region. International Journal of Thermophysics , Vol. 20, No. 5, 1339-1366.

[27] F. Volklein, F, and D.-P. E. Kessler, 1987. Methods for the measurement of thermal conductivity and thermal diffusivity of very thin films and foils. Measurement Vol 5 No 1 , 38-45.

[28] H. S. Jaeger, 1986. Conduction of Heat in Solids. New York: Oxford University Press.

[29] http://en.wikipedia.org/wiki/Nickel.

[30] http://en.wikipedia.org/wiki/Strengthening_mechanisms_of_materials.

[31] http://instserv.com/rmocoupl.htm

[32] http://www.appliednanotech.net/tech/cnt_displays.php

[33] http://www.efunda.com/designstandards/sensors/thermocouples/thmcple_theory.cfm

[34] http://www.engr.ucr.edu/~cdames/research.html#1_2_and_3_omega_methods_for_thermal

[35] http://www.omega.com/temperature/z/pdf/z021-032.pdf

[36] http://www.omega.com/Temperature/pdf/TC_CJ_REF.pdf

[37] H. Wang, M. Sen, 2009. Analysis of the 3-omega method for the thermal conductivity measurement. International Journal of heat and Mass Transfer , 2102-2109.

[38] J. P. Holman, 1994. Experimental Methods for Engineers Sixth Edition. New York: McGraw Hill, Inc.

[39] O. M. Corbino, 1910. Thermal oscillation in lamps of thin fibers with alternating current flowing through them and resulting effect on the rectifier as a result of the presence of even-numbered harmonics. Phys. Z. 11, 413-417.

[40] W. A. Wakeham, 1999. Thermal Conductivity Measurement. CRC Press LLC.

[41] W Wu, J. Shen, P. Banerjee and S. Zhou, 2010. Core-shell hybrid nanogels for integration of optical temperatur-sensing, targeted tumor cell imaging, and combined chemo-photothermal treatment. Biomaterials , 1-12.